Applied Energy 302 (2021) 117526

Contents lists available at ScienceDirect

Applied Energy

journal homepage: www.elsevier.com/locate/apenergy

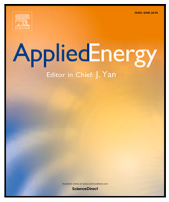

Impact of fuel cell range extender powertrain design on greenhouse gases and NO_X emissions in automotive applications

J.M. Desantes, R. Novella *, B. Pla, M. Lopez-Juarez

CMT-Motores Térmicos, Universitat Politècnica de València, Camino de vera s/n, 46022 Valencia, Spain

ARTICLE INFO

Keywords:
Hydrogen
Fuel cell vehicle
Range-extender
Driving cycle
Sizing
LCA

ABSTRACT

Fuel cell (FC) technologies for mobility are gaining interest as promising options to decarbonize the transport sector in line with the current progress towards the H_2 economy. Previous studies show how the fuel cell range extender (FCREx) powertrain architecture can offer flexible and efficient operation along with the potentially low total cost of ownership (TCO) in passenger car applications. Cradle-to-grave emissions of these vehicles have not been estimated, nor their variation with the components sizing or the H_2 production pathway analyzed. In this study, the life cycle assessment (LCA) and sizing methodologies were combined to address these knowledge gaps. The design spaces were generated by varying the FC maximum power, the battery capacity and the H_2 tank capacity and by simulating the resulting designs with the WLTC 3b driving cycle. Then, the lifetime H_2 and energy consumption results and design parameters were calculated and used as inputs to estimate the greenhouse gases (GHG) and NO_X emissions on the manufacturing and fuel production cycles. From the results, it was proven how considering steam methane reforming (SMR) with carbon capture and storage (CCS) as the H_2 production pathway could decrease by 60% and 38% GHG-100 and NO_X emissions respectively, with respect to electrolysis where electricity is generated with the EU mix. The optimum design, in terms of emissions, was found to be with low-moderate battery capacity and moderate-high FC maximum power in contrast to the optimum design for performance, which had high battery capacity and high FC stack power.

1. Introduction

The use of H_2 in fuel cells (FC) for mobility and power generation application has been continuously growing during the last decade since it is an effective enabling technology for the decarbonization of these sectors [1]. Apart from H_2, there are different choices to also fulfill this objective: batteries and e-fuels. Batteries are more efficient than fuel cells, but their low energy density limits the battery-electric vehicles' (BEV) range capabilities (200–400 km), imply prohibitive costs for those with high range and have excessively long charging time [2]. E-fuels can be generated from H_2 and captured CO_2, thus enabling long-range displacements and CO_2-neutral emissions [3]. However, CO_2 and other emissions are released in-situ, thus increasing local pollution in cities. In contrast, H_2 FC vehicles (FCV) enable long-range displacements (500–800 km), high-efficiency energy utilization, fast refueling, low cradle-to-grave emissions and pollution decentralization [4].

The tank-to-wheel emissions produced by H_2-fueled engines or FC are mostly composed of H_2O vapor, which allows the decentralization of emissions. Nonetheless, due to certain factors such as the lack of infrastructure, the difficulties of H_2 distribution and the multiple production pathways available to produce H_2, the cradle-to-grave emissions when using H_2 as an energy vector may be significant. Depending on the production pathway, H_2 can be classified according to different colors: black when it is produced from electrolysis whose energy has been obtained from fossil fuels, gray when it is obtained from steam methane reforming (SMR), blue when the production pathways are either electrolysis from nuclear power or SMR with carbon capture and storage (CCS) technologies, and green when it is obtained from electrolysis with electricity generated from renewable sources. Among this spectrum, green H_2 implies the lowest cradle-to-grave emissions, yet it requires large infrastructure and is not achievable in the short-term on a large scale. Furthermore, in terms of costs, blue H_2 is a significantly cheaper option than green H_2, thus being the optimal production pathway to extend the use of H_2 until enough infrastructure to produce green H_2 is developed [5]. Due to the unfeasible short-term application of green H_2, this study only considers black, gray and blue H_2. Furthermore, the choice of considering blue H_2 rather

* Corresponding author.
E-mail address: rinoro@mot.upv.es (R. Novella).
URL: http://www.cmt.upv.es (R. Novella).

https://doi.org/10.1016/j.apenergy.2021.117526
Received 23 February 2021; Received in revised form 27 July 2021; Accepted 1 August 2021
Available online 13 August 2021

than green H_2 was motivated to avoid any bias in the present study towards fuel cell vehicles since two energy sources are considered to power FCVs in this study: H_2 and electricity. As such, it could be argued that considering green H_2 and electricity from the common mix (EU, USA, China, ...) would result in a biased study since the additional renewable energy required to produce H_2 could be used to decarbonize the electricity mix, thus making the use of electricity produce lower emissions than the use of H_2. Even though green H_2 is not considered as the main production pathway due to the reasons previously explained, an appendix was added to understand the effect of considering an even lower-emission production pathway than H_2. The emissions associated with each type of H_2 were compared to understand the implications considering high-emissions production pathways.

In recent years, several FCV has been released to the market (Honda Clarity, Toyota Mirai, and Hyundai Nexo). Shallowly, the architecture of these vehicles is composed of a low-capacity battery with a high-power FC system. This architecture is mainly designed to use the FC system to power the vehicle during most of the operation with the battery as a supporting power source. Nevertheless, this configuration is not suitable for the current scenario with a such low number of refueling stations worldwide [6]. In previous work, the authors of the present study proposed the previously unexplored use of FC systems as a range-extender (FCREx) in passenger vehicles [7]. This architecture has previously been considered for other types of vehicles such as trucks, captive fleets, or city buses, yet not for light-duty passenger cars. FCREx configuration consists of a moderate-capacity battery together with a moderate-to-high FC stack maximum power and offers many advantages such as flexible operation (BEV and FCREx modes), significantly lower total cost of ownership (TCO), potentially lower cradle-to-grave emissions and lower energy consumption, compared to conventional FCV [4,7].

Other research lines include alternative FCV architectures such as those with fuel processors to obtain H_2 from liquid fuels such as ethanol [8] to extend even further the vehicle range given the extra consumption of auxiliary components [9]. Although these alternative architecture have been proved to be interesting to extend the range of FCVs, they require additional components and lower-capacity batteries than the architecture proposed in this study, which follows the range-extender concept.

The sizing studies of passenger FCV are usually limited to low-capacity batteries of super-capacitors [10] ($\leq$5 kWh) and high-power FC stacks [11]. In contrast, for the sizing of a FCREx vehicle, the ranges of battery capacity and FC stack power must change and the H_2 tank capacity must be included since, along with the battery, is the main source of energy and affects the range of the vehicle. As such, for FCREx sizing studies, the sizing parameters must be the battery capacity, the FC stack maximum power and the H_2 since they have a direct impact on cradle-to-grave emissions, electricity and H_2, vehicle range, and TCO.

The state-of-the-art for FCREx is represented by limited literature and the only application of FCREx architecture to heavy-duty vehicles or captive fleets. In the literature regarding the use of the FCREx configuration for city buses, Xu et al. [12] analyzed different designs of FCVREx in terms of costs and range for city buses using the CDCS (charge depleting and charge sustaining strategy). They concluded that to minimize H_2 in FCVREx the priorities are in order: reducing auxiliary power, braking energy recovery, increase FC stack efficiency and decreasing battery losses. In further studies [13], they used a two-step algorithm based on dynamic programming to obtain a quasi-optimal solution to the sizing problem. With this approach, they concluded that a battery of 150 Ah and an FC system maximum power output of 40 kW were optimal for fuel economy and systems durability for an FC city bus.

Apart from city buses, this architecture has also been considered for captive fleets, where the refueling and recharging infrastructure is always close to the operating zone of the vehicle, and trucks. In this sense, Wu et al. [14] used convex programming to solve the sizing problem for urban logistics FCVREx. They concluded with an optimum battery capacity of 29 kWh and an FC stack maximum power and usage dependent on the hydrogen price but did not include the mass of hydrogen stored as a variable for the sizing since urban logistics vehicles do not need a high range. They followed their research by considering the FCVREx architecture in trucks [15], showing that convex programming methods could provide minimal H_2 consumption in 8*CHTC-HT and 7*C-WTVC Chinese truck driving cycles.

As commented before, other authors have also considered the sizing of FCV with conventional configurations. Following this line of research, Gaikwad et al. [16] used a pinch-based analysis for sizing the FC system together with a supercapacitor considering the WLTC class 3 driving cycle, concluding that the FC size must be at least equal to the average power demand for a given cycle while the supercapacitor capacity is only limited to a minimum value if regenerative braking is considered. Hu et al. [17] performed a sizing analysis of the Lithium battery of an FCV passenger car with multi-objective real-time EMS considering fuel economy and system durability to reduce the life cycle cost. However, the maximum battery capacity considered was 24 Ah, not enough to provide normal operation in the pure-electric mode for a reasonable range. Therefore, it cannot be considered an FCVREx.

There has been extensive work in the last decade about the use of life cycle assessment (LCA) methodologies to estimate the cradle-to-grave emissions of H_2-based fuels and technologies. LCA studies are an important tool that serves as a base of comparison to understand the environmental impact of technologies in different sectors [18], scenarios [19], and even costs [20]. Nonetheless, this LCA study focuses on estimating the cradle-to-grave emissions rather than in costs given the current growth of the H_2-related technologies and the huge variation in their costs during the previous and following years. None of the studies focused on LCA for H_2 technologies consider the use of FCREx architecture for passenger vehicles. The recent research found in the literature shows how e-fuels (or H_2-based synthetic fuels) have gained interest due to the neutral CO_2 emissions their usage implies [21]. Nonetheless, it has been proved that the use of H_2 produced through electrolysis from renewable sources could decrease the greenhouse gas emissions (GHG) significantly more than e-fuels while if it is produced through SMR the H_2 cost could be lower than the e-fuels cost [22]. In this regard, the direct use of H_2 in FC has also been proven to have clear advantages in terms of well-to-wheel efficiency, GHG-100 and other pollutant emissions, and fuel cost for light-duty passenger vehicles [23].

The studies regarding the emissions associated with the H_2 value chain are mostly focused on a very specific part of the cradle-to-grave process such as H_2 production [24] and distribution [25], FC stack production and recycling [26], and storage [27]. Those focused on the general cradle-to-grave process show how FC vehicles could significantly reduce the GHG emissions with respect to conventional ICEV [28] and even BEV [4] if H_2 is produced through SMR with CCS. In the literature, only Dimitrova et al. [29] considered the environmental impact of a vehicle with a solid-oxide FC (SOFC) operating as a range-extender. Nevertheless, none of them considers the use of Proton Exchange Membrane FC (PEMFC) as a range-extender in FCREx vehicles nor the variation of the environmental impact of FCREx vehicles with design and H_2 production pathway.

1.1. Knowledge gaps

In light of the previous studies, some conclusions can be extracted to provide an idea of the knowledge gaps in the literature:

1. The studies about the use of FCREx architecture for light-duty passenger vehicles are limited since most of the research has been focused on the use of this configuration of heavy-duty vehicles or captive fleets.

2. No data was found about the lifetime H_2 and overall energy consumption of FCREx passenger vehicles nor about how they change with the sizing of the battery, the H_2 tank capacity and the FC stack maximum power.
3. The environmental impact, in terms of GHG and NO_X emissions, of FCREx vehicles with PEMFC technology has not been assessed yet. Not to mention the application of this architecture to passenger vehicles.
4. Most of the studies focus on a specific vehicle or design but do not consider the variability of the environmental impact with the sizing of the components. There is no information about how the cradle-to-grave emissions of FCREx vehicles change with the components sizing. The combination of LCA with sizing methodologies is a novelty itself.
5. There are no studies about how the cradle-to-grave emissions of a vehicle with two power sources comprising the powerplant such as FCREx change with the H_2 production pathway.
6. There is a lack of research about how the cradle-to-grave emissions of an FCV change if it is designed for a different target range.
7. The performance of FCREx has only been assessed in terms of H_2 consumption, but no data about the optimum design in terms of cradle-to-grave emissions is available. Also, there is no information about whether the optimum FCREx design in terms of performance coincides with the optimum design that minimizes cradle-to-grave emissions.

In conclusion, the literature regarding the sizing of FCREx is still limited, particularly for passenger vehicles, and mostly omits the fundamental behavior and optimization of the FC system while do not pay attention to the cradle-to-grave emissions implication. Also, there is no study combining both sizing and LCA methodologies to understand the design implications both in terms of emissions, lifetime fuel or energy carriers consumption, and performance. This study combines both LCA and sizing methodologies to understand the impact of FCREx design on performance and emissions and to provide recommendations about the future design choices for this type of FCV.

2. Contribution and objectives

This study intends to address all the knowledge gaps listed above. In order to do so, the LCA and sizing methodologies are combined. With the sizing methodology, the H_2 and energy lifetime consumption are calculated for FCREx passenger vehicles, thus allowing to analyze the energy carriers utilization and its variation with the components sizing (knowledge gaps 1, 2). With the design spaces obtained from this combination in terms of GHG-100 and NO_X emissions, it is intended to analyze and understand how the cradle-to-grave, fuel cycle and manufacturing cycle GHG-100 and NO_X emissions change with the FCREx design, the target range and the H_2 production pathway (knowledge gaps 3, 4, 5 and 6). Special attention is paid to blue H_2 since it is the lowest pollutant production pathway that is feasible in the short term. In this case, the relative emission-production of the vehicle manufacturing and fuel production cycles with respect to the total emissions are analyzed to understand the relative importance of each cycle of the cradle-to-grave process to minimize GHG-100 and NO_X emissions. With the data at hand, the optimum FCREx design in terms of emissions and consumption are compared to understand if they overlap or are different in order to understand which factors affect the sizing of the optimum FCREx design (knowledge gap 7). Finally, it will be possible to elaborate recommendations for the FCREx design process-based, not only on performance but also on cradle-to-grave emissions. These recommendations are not only focused on how the FCREx should be designed, but also on how it should be taken action on the fuel production and vehicle manufacturing processes to minimize the cradle-to-grave emissions of FCREx efficiently.

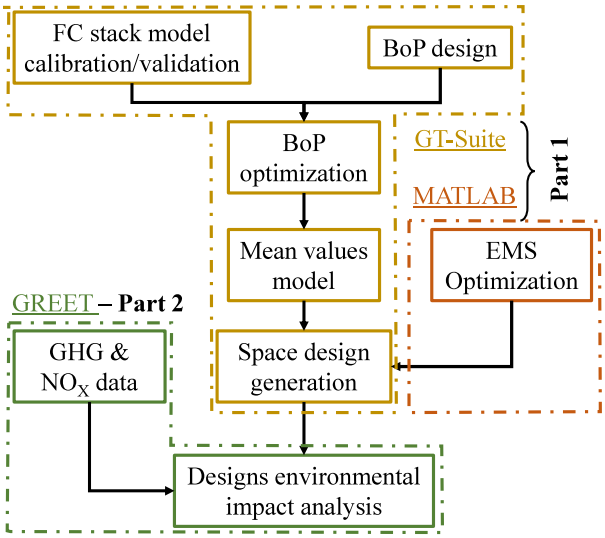

Fig. 1. Methodology schematic, simulation tools and differentiated parts.

3. Methodology

In this section, the methodology applied to perform this study is described. It can be divided into two different parts: the FCREx modeling (part 1) and the LCA (part 2) methodologies. Fig. 1 shows a schematic of the methodological procedure followed. Albeit the two parts are equally important to obtain the results of this study, the explanation of the FCREx model is simplified since previous studies contain extensive and detailed information about the FCREx modeling procedure [7]. For the LCA methodology, FCREx design and H_2/electricity consumption data were used as inputs from the simulations performed following the first part of the methodology.

3.1. FC vehicle model description

This model was developed in previous studies to understand the performance in terms of consumption and range of FCREx architecture in WLTC 3b cycles with different designs [7]. The model was implemented in the commercial simulation platform GT-Power. This software is extensively used in the automotive industry to simulate thermo-fluidynamic systems by numerically solving the mass, energy, species and momentum conservation equations, among others. The FC model was calibrated to experimental results using genetic algorithms with an overall error lower than 2% (Fig. 2). The experimental data used were extracted from [30,31]. They consisted of the polarization curves of a 20 kW FC stack at the following conditions:

- T_{stack} = 346 K & $p_{cath\ in}$ = 1.3 bar
- T_{stack} = 346 K & $p_{cath\ in}$ = 2.5 bar
- T_{stack} = 305 K & $p_{cath\ in}$ = 1.3 bar

Furthermore, the behavior of the model to cathode stoichiometry was also validated with data from the same papers. Unlike other studies, the FC model was validated at different operating conditions of pressure, temperature and stoichiometry so that the results obtained from simulations such as driving cycles, where the FC temperature and the air management are constantly changing with the operating conditions, are meaningful and representative.

Once the FC stack model was validated, it was integrated into a fully scalable balance of plant (BoP), thus forming an FC system (Fig. 3) which includes: a H_2 recirculating pump, an electric compressor, a cooling circuit, a heat exchanger after the compressor and a cathode inlet humidifier. This BoP was designed and optimized to maximize the

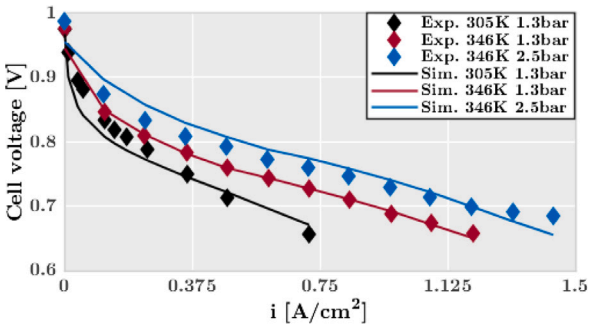

Fig. 2. Fuel cell model validation results and comparison against experimental data [7].

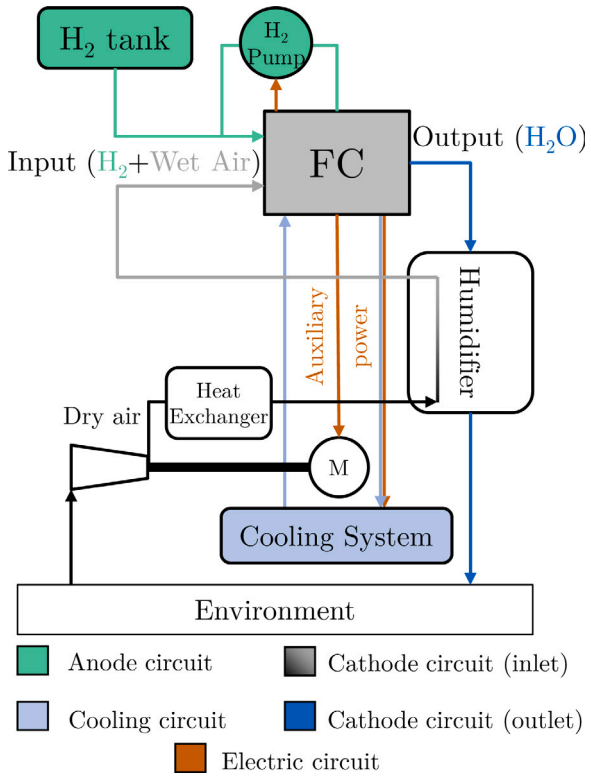

Fig. 3. Fuel cell system sketch including the stack and all the components of the balance of plant: e-compressor, H_2 tank, anode recirculation, cooling system, cathode humidifier and heat exchanger [7].

efficiency of the FC system in previous studies [7], reaching a maximum efficiency close to 60% including the losses associated with the DC–DC converter before the electrical power output of the FC system and the consumption of all the components of the BoP. For further information about the BoP components characteristics and optimization procedure, the reader can refer to previous studies [7]. In order to ensure the FC stack integrity and correct operation, some restrictions were imposed in the BoP management strategy:

- Anode stoichiometry was always kept close to 3 by controlling the H_2 in the anode recirculation loop to avoid anode starvation that may lead to the FC stack malfunctioning or severe degradation.
- Anode pressure was kept 0.3 bar above cathode pressure to improve H_2 diffusion. Thus, the control strategy was designed so that the difference in pressure was kept close to this 0.3 bar also to avoid structural damage and preserve the FC stack mechanical integrity.
- Cathode inlet relative humidity (RH) was kept, when possible, to 80% to ensure sufficient membrane humidity.
- Cathode inlet pressure was kept always over 1.2 bar to overcome the pressure loss in the FC stack and below 2.5 bar to preserve the mechanical integrity of the FC stack.
- The air management strategy was designed so that the cathode stoichiometry was kept over 1.8 to avoid starvation. This value is lower than the target anode stoichiometry since the compressor consumption is significantly higher than the H_2 pump required power. As such, to maximize the FC system efficiency the target cathode stoichiometry had to be lower.

The electronic architecture of the FCREx was indirect. This means that DC–DC converters are used at the output of the FC system and the battery so that the FC system can be downsized and protected from the electrical fluctuations that may come from the bus system [32]. Also, an AC–DC transformer was connected to the electric motor that produces the brake power (dimensioned for 120 kW of maximum power). The electric efficiency of each transformer was 95%. The battery pack was a Li-Ion battery composed of 100 cylindrical cells to provide enough power when required, and a variable number of parallel cells defining the battery capacity. Each cell had a nominal voltage of 3.6 V and a nominal capacity of 3.35 Ah. The cells were modeled using an equivalent electric circuit (RC) whose open-circuit voltage and resistance (losses) depend on the state-of-charge. The battery temperature evolution was checked using a lumped thermal mass model to ensure the battery operating conditions were kept within safety limits.

The vehicle body was SUV-type. This body was chosen so that there is enough space in the vehicle to fit all the systems in the sizing procedure at the expense of reducing the available space in the trunk. The body characteristics were selected based on the Hyundai Nexo FCV technical data [33]. The dry weight of the FCREx designs without the FC system, the battery and the H_2 tanks was set as 1400 kg, with a drag coefficient of 0.329 and a frontal area of 2.58 m^2. The aerodynamic parameters were constant among designs since they could be fitted inside the vehicle without external modifications.

3.1.1. Mean values model

As explained in previous work [7], the computational time of running a simulation of a complete FCREx model in a driving cycle such as the WLTC 3b cycle is around 4 h. The design space calculated for this and previous studies consisted of a significant number of designs to consider all the possible combinations of the three parameters varied during the sizing and to minimize any possible discretization/interpolation error in the design spaces. With these boundary conditions, carrying out the required simulations for this study would require around 10 months. Therefore, in order to reduce the computational time, the FC stack model was simplified to a mean values model using data from steady-state simulations of the complete model, thus decreasing the computational time from 4 h to 50 s per driving cycle simulation. Due to the steady-state nature of the model, in contrast with the dependence of the FC stack performance to dynamic behavior, a small deviation with respect to the complete model was found in previous studies [7]. Nonetheless, the results produced with this model are based on validated results of a complete FC system model and consider the change in the optimized BoP operation with the requested load to the FC stack. As such, it can provide much higher fidelity results than other approaches used in the literature (as explained in the introduction section) despite the simplification of the inefficiencies associated with the FC stack transient behavior.

3.1.2. Energy management strategy

The energy management strategy (EMS) in vehicles with different power sources such as FCVs is critical for the efficient operation of the systems [34]. In the case of FCREx vehicles, the power sources are the FC system and the battery. Therefore, to optimize the EMS

Table 1
Energy management description and main characteristics.

Control input (u)	Fuel cell power	P_{FC}	
State	Energy in the battery	E_b	
Objective/Cost function	H_2 consumption minimization	$J = \int_{t_0}^{t_f} P_f(u(t), t)\,\mathrm{d}t$	(1)
Constraint	Battery charge sustaining	$\int_{t_0}^{t_f} P_b\left(u(t), E_b(t), t\right)\mathrm{d}t = 0$	(2)
Algorithm	Pontryagin's Minimum Principle (PMP)		

it is necessary to find the sequence of power split that complies with the systems requirements with minimum cost [35]. In a study like the present one, where different designs whose optimum EMS is different are compared, ensuring that each design operates with the best performance is mandatory to eliminate any bias. Optimal control (OC) is a tool developed specifically for benchmarking studies since it provides the optimal power split sequence for every powertrain considered. This tool was used to ensure that the designs are compared in the best-case scenario [36].

The overall description of the EMS optimizer can be found in Table 1. The cost function J (Eq. is the result of integrating along the simulation time the H_2 power consumed (P_f) which is controlled through the control variable u. In the case of FCREx vehicles, the driving mode that uses the FC system must ensure that the energy in the battery (E_b) or the state of charge of the battery (SOC) is sustained. As such, this condition is imposed as a constraint for the EMS (Eq.) by means of the power consumed by the battery (P_b) integration.

In order to solve the OC problem, Pontryagin's Minimum Principle (PMP) was applied. It allows solving an integral optimization problem as a set of differential optimization problems. The PMP states the necessary conditions for optimal trajectories in the control and state of a dynamic system. In particular, PMP applied to the case at hand implies:

$$H\left(u^*, E_b^*, \lambda^*, t\right) \leq H\left(u, E_b^*, \lambda^*, t\right) \forall u \in U, t \in [t_0, t_f] \tag{3}$$

where u^* and E_b^* are the optimal trajectories of the control and state of the problem and H is the Hamiltonian function, defined as:

$$H = P_f - \lambda \dot{E}_b = P_f(u(t), t) + \lambda(t) P_b\left(u(t), E_b(t), t\right) \tag{4}$$

According to the PMP, the dimensionless co-state λ varies with the evolution of H respect to the state E_b:

$$\dot{\lambda} = \frac{\partial H}{\partial E_b} \tag{5}$$

Combining with Eq. (4):

$$\dot{\lambda} = \lambda \frac{\partial P_b}{\partial E_b} = \lambda P_{batt} \frac{\partial\left(P_b / P_{batt}\right)}{\partial E_b} \tag{6}$$

The ratio P_b/P_{batt} represents the inverse of the battery efficiency (power consumed over power provided). If the battery state of charge is controlled around its design range, the variation of the efficiency with its energy level E_b is small. Therefore, according to Eq. (6), the co-state λ can be assumed constant [37]. This implies that the OC problem can be solved with the PMP by iteratively looking for the value of λ that fulfills the required constraint (Eq. (2)). A more detailed description of the EMS optimization algorithm can be found in previous studies [7].

3.1.3. Sizing: design spaces generation

Regarding the sizing procedure, three key design parameters were varied to cover a wide range of FCREx designs: FC stack maximum power output, H_2 tank capacity, and battery capacity. Among these parameters it was shown how the former had the lowest effect on range but the greatest effect on H_2 consumption while the other two had significant effect on range and overall energy consumption [7]. The limits within which these parameters were varied are:

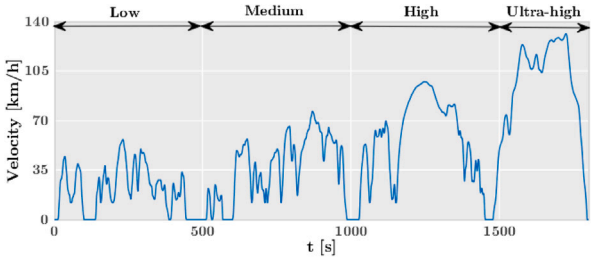

Fig. 4. Worldwide harmonized Light vehicles Test Cycles (WLTC) 3b cycle description. Low, medium, high and ultra-high dynamics regions are indicated.

- FC stack maximum power $\in$ $[20, 100]$ kW
- H_2 tank capacity $\in$ $[1, 5]$ kg
- Battery capacity $\in$ $[30, 60]$ kWh

The lower limit for the battery capacity (30 kWh) was chosen from preliminary simulations so that it ensures enough operable range in the battery mode with such vehicle body and systems. The mass and volume of each system was added to the total mass and varied for each design, i.e., two different simulations with different FCREx systems sizing have different weight and has influence over the vehicle consumption. The volume was also estimated to ensure that the H_2 tank and the battery could fit in the rear part of the vehicle at the expense of trunk space. The data used in the sizing are in Table 2.

The data about H_2 and electricity consumption were estimated by simulating the FCREx vehicles with the WLTC 3b driving cycle, corresponding to a power-to-mass ratio ≥34 for all the possible designs considered with an electric motor of 120 kW. The WLTC 3b driving cycle is characterized by four different regions of operation: low, medium, high, and ultra-high dynamics regions (Fig. 4). Even though this comprises a significant number of driving conditions, it is still not fully representative of real driving. Given the designs and vehicle considered in this study, the brake power consumption in this cycle is around 12.4 kWh/100 km. The range was estimated by first operating the vehicle with the battery until SOC = 0.3, then the operation in FCREx mode following the battery charge-sustained criteria explained in Section 3.1.2 with optimum EMS until H_2 depletion, followed by operation with the battery until charge depletion. The criteria of considering the battery SOC = 0.3 for FCREx mode is based on the philosophy behind range-extender vehicles, whose main operation could be in battery mode until low SOC is achieved when the range-extender powerplant is activated to enable charge-sustaining operation. Considering higher SOC would lead to lower battery losses and thus to the under-prediction of H_2 consumption.

3.2. Life cycle assessment

This section, together with its corresponding subsections, is focused on explaining the LCA methodology after obtaining the H_2 and electricity consumption data as inputs (Fig. 6). Most of the emissions-related data were obtained from the GREET® model v2019 as well as from other data sources in the literature. The emissions data for each H_2 production pathway are those obtained [4] for the scenario with the

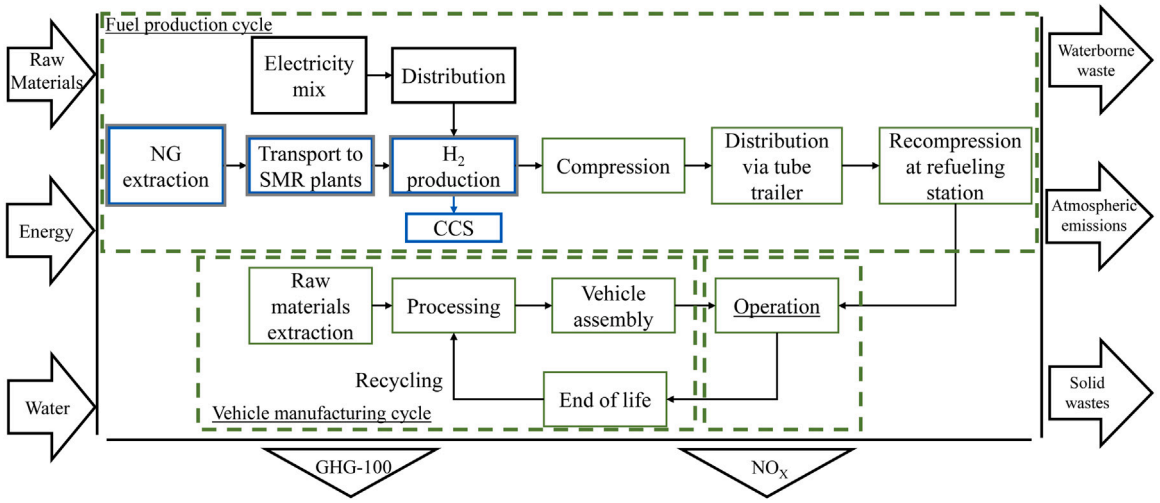

Fig. 5. System boundaries and elementary flows for the cradle-to-grave process considering electrolysis, SMR and SMR with CCS as the H_2 production pathways. Processes unique to electrolysis production pathway are in **black**, those unique to SMR are in gray, and those unique to SMR with CCS are in blue.

Table 2
Data used to calculate the mass and volume of the systems [38–41]. These data were integrated into the FCV model to increase its weight depending on the powertrain design.

System	Data used to estimate Mass - Volume
FC system	Linear correlation: • Estimated 175 kg and 286 l for a 30 kW system • 250 kg and 614 l for a 70 kW system
H_2 tank	0.045 kg H_2/kg system 0.030 kg H_2/l system
Battery	220 Wh/kg 600 Wh/l

current EU electricity mix so that the results are representative of the short-term scenario. In this LCA analysis, all the pathways involved in the cradle-to-grave process were considered, i.e., the LCA analysis comprises the fuel production cycle, the vehicle manufacturing cycle and the operation cycle.

3.2.1. System boundaries

A schematic of the system boundaries and the elementary flows considered in this study for the cradle-to-grave process considering electrolysis, steam methane reforming (SMR) and SMR with carbon capture and storage (CCS) is shown in Fig. 5. In the present study, despite many outputs of the cradle-to-grave process such as waterborne waste and other emissions such as SO_X were calculated, the analysis only considers the GHG-100 and NO_X emissions as the system outputs.

3.2.2. Functional unit

The functional unit in this study was changed according to the process under analysis to improve readability. The functional unit for the emissions in the vehicle manufacturing cycle was 1 unit of such vehicle. For the emissions produced in the fuel production cycle, the functional unit was 120,000 km of vehicle average useful life. This life was set slightly lower than the commonly used for hydrocarbon-fueled ICEV (150,000 km) since the batteries and FC durability are lower. Finally, in the cradle-to-grave process, the functional unit was both 1 unit of vehicle and 120,000 km of useful life, i.e., the total emissions during the vehicle life.

In the case of Section 3.2.4, where the life cycle inventories are presented, in the case of the fuel production cycle, the emissions are given in terms of kWh of energy source, since different energy sources are being considered (H_2 and electricity). These values are then multiplied by the total life H_2 and electricity consumption (Fig. 6) to obtain the fuel production cycle emissions along the whole vehicle life.

The values of Table 4 are given as a function of the component sizing parameter (kWh of energy stored in the case of the battery and the H_2 tank and kW of maximum stack power for the FC system) so that they can be directly converted into emissions by knowing the sizing parameters.

3.2.3. Impact categories

In the present study, GHG-100 was the main impact category considered since the main objective of extending the use of FCV is to reduce the global warming impact of the transport sector. GHG-100 is an impact category that represents the global warming potential of different gases over a period of time of 100 years. According to this category, each greenhouse gas has assigned a value of global warming potential (GWP) that represents the relative effect on global warming of 1 g of such gas compared to the effect of 1 g of CO_2. The GHG-100 were calculated by taking into account CO_2, CH_4 and N_2O emissions with their GWP of 1, 28, and 265 kg CO_2 equivalent, respectively [42]:

$$\text{GHG-100} = m_{CO_2} \cdot GWP_{CO_2} + m_{CH_4} \cdot GWP_{CH_4} + m_{N_2O} \cdot GWP_{N_2O}$$

where m_{CO_2}, m_{CH_4} and m_{N_2O} are the CO_2, CH_4 and N_2O mass emissions, respectively.

Furthermore, NO_X emissions, although they are not an impact category, were also calculated due to the harmful effects they pose to human health, as well as, their effect on ozone depletion at high altitudes and ozone generation at low altitudes.

3.2.4. Life cycle inventory

The life cycle inventory (LCI) data was mainly extracted from GREET® v2019 model, although some data was corrected and added from the literature. This model is extensively used in the automotive industry and has been the source of data of many studies [14,43–45]. In this section, unless otherwise specified, the presented data was obtained from GREET® model.

The life cycle inventory can be separated according to the part of the cradle-to-grave process it is used to provide data: fuel production cycle, vehicle manufacturing cycle and operation cycle (Fig. 5).

Fuel production cycle LCI

The fuel production cycle comprises all the processes from the raw material extraction until the vehicle refueling. It can be also referred

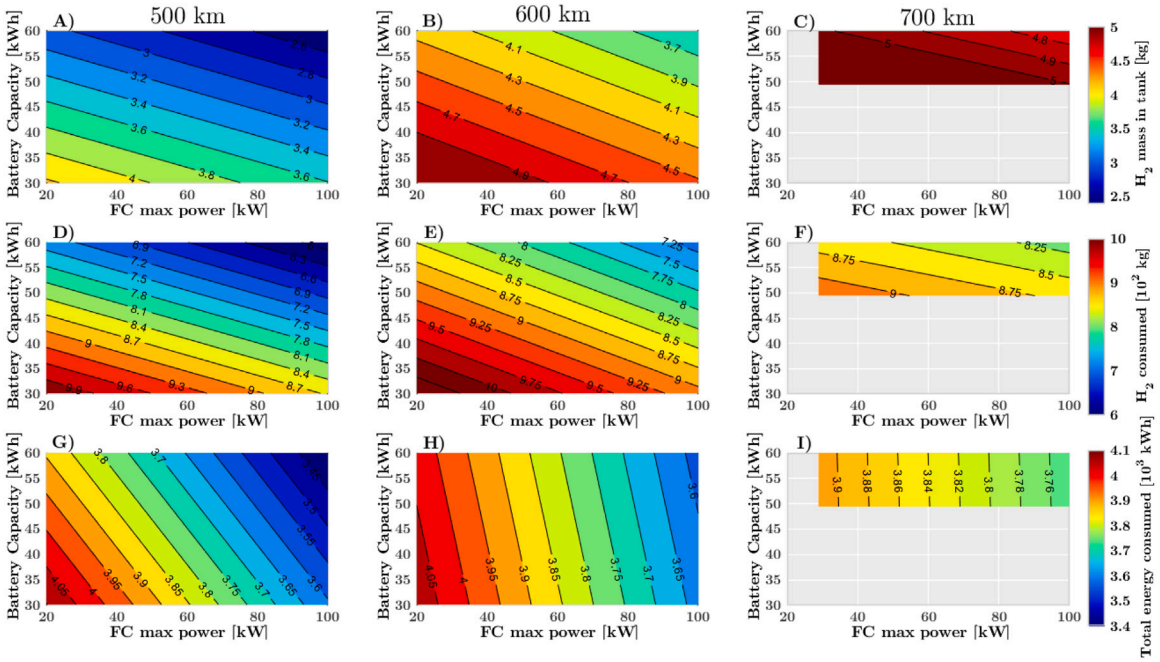

Fig. 6. Design spaces for 500, 600, and 700 km of range FCREx. Contours show: H_2 mass in tank to achieve the target range (1st row), H_2 consumed along the whole life (2nd row), and NO_X total energy consumed along the whole life, including H_2 and electricity in the operation cycle (3rd row).

Table 3
Fuel cycle LCI data: GHG-100 and NO_X emissions. Functional unit is kWh of energy source (H_2 or electricity produced).

Production pathway	GHG-100 emissions [kg CO_2 eq./kWh]	NO_X emissions [kg/kWh]
H_2-Electrolysis (**black**)	0.489	$5.1 \cdot 10^{-4}$
H_2-SMR (gray)	0.343	$1.5 \cdot 10^{-4}$
H_2-SMR w/ CCS (blue)	0.111	$2.0 \cdot 10^{-4}$
Electricity	0.316	$3.6 \cdot 10^{-4}$

Table 4
Vehicle manufacturing cycle LCI: GHG-100 and NO_X emissions. Emissions given per unit of sizing parameter.

System	GHG-100 emissions [kg CO_2 eq.]	NO_X emissions [kg]
Battery capacity [/kWh]	26.07	$3.9 \cdot 10^{-2}$
FC stack power [/kW]	7.84	$8.7 \cdot 10^{-3}$
H_2 tank capacity [/kg H_2]	424	$4.9 \cdot 10^{-1}$
H_2 tank capacity [/kWh]	12.73	$1.46 \cdot 10^{-2}$

as the well-to-tank process. As explained before, three different H_2 pathways were considered: electrolysis with electricity from the current EU electricity mix, SMR and SMR with CCS. In these three pathways, the H_2, after being produced, is compressed and distributed via tube trailers to be re-compressed at the refueling station (Fig. 5). These production pathways along with the distribution procedure and the EU electricity mix were considered since they represent the closest-to-present scenario. Green H_2 and distribution via pipeline are not considered due to the large infrastructure it needs to be feasible at a reasonable scale, which means they are not feasible at the short-term. In contrast, producing H_2 with distributed electricity or through SMR with or without CCS is relatively immediate since most of the H_2 at the present is produced through SMR, whose plants can be adapted to include CCS strategies. In the case of CCS technology, a CO_2 sequestration capacity of 90% was assumed, based on the literature data [46].

Apart from H_2, there is another energy source in FCREx vehicles: electricity stored in the battery. The GHG-100 emissions per kWh of electricity were obtained from [47] assuming a 6.5% of distribution and transmission losses [48]. Table 3 shows the GHG-100 and NO_X emissions per kWh of energy source for each production pathway, considering all the processes described. Total emissions were calculated with a refueling efficiency of 1.

Vehicle manufacturing cycle LCI

The emissions produced in the vehicle manufacturing cycle are subjected to significant changes in this study since the vehicle design changes. The emissions associated with the production of each component were scaled to those corresponding to a 1400 kg vehicle body. The vehicle manufacturing cycle comprises the manufacturing of mechanical components (transmission system, chassis, traction electric motor, electronic controller, vehicle body and vehicle tire replacement), the assembly, disposal and recycling (ADR) processes, the fluids manufacturing (brake, transmission, coolant, windshield and adhesives), the battery (NMC111 Li-ion), the FC system and the H_2 tank (type IV carbon fiber for 700 bar). The data associated with the recycling of the FC system and the H_2 were not included since emissions associated with the FC stack recycling are negligible [49] and there is not enough data in the literature about the emissions produced during the recycling of H_2 high-pressure tanks. The emissions data for the components whose specifications change in the design spaces (sizing) are given in Table 4 per unit of sizing parameter. The sizing parameters, or those controlled to modify the components sizing, are the FC stack maximum power (kW) the battery capacity (kWh) and the H_2 tank capacity (kWh of H_2 or kg of H_2).

The raw materials (inputs in Fig. 5) considered for the manufacturing of such vehicles were steel, aluminum, magnesium, zinc, copper wires, glass, plastic product, styrene–butadiene rubber, carbon-fiber-reinforced plastic, lithium and other vehicle materials. The emission associated with the processing of raw materials and the extraction of elementary materials such as sand water, bauxite ore, zinc ore, etc,

were considered while those generated during the transport of such materials to the manufacturing plants were neglected [50].

Operation cycle LCI

The operation cycle can also be called the tank-to-wheel process. Different from conventional ICE vehicles, the emissions produced by FCV and their effect on the environment are minimal. The only significant tank-to-wheel emission of FC systems is H_2O. In this study, the H_2O emissions of the FCREx vehicles when operating in the range-extender mode and their effect on global warming were considered. For that purpose, the effective global warming potential of water was set as $5{\cdot}10^{-4}$ kg CO_2 eq. [51]. This value is the result of two contrary effects of near-surface emitted water vapor: the effect of water as a GHG-100 emission and the decrease in temperature due to the formation of low-altitude clouds that increase the atmosphere reflectance.

4. Limitations of the study

Before presenting the results obtained and the discussion, it is important to highlight the limitations of this study derived from the hypotheses and methodologies applied:

- The results of this study are applicable to SUV-type passenger vehicles since they represent an important fraction of the vehicle fleet and their size enables the coexistence of moderate-capacity batteries together with FC systems.
- Europe and United States technology level are assumed to be similar (GREET® model) while the main difference is the electricity mix.
- The emissions produced in the manufacturing processes of the machines and devices used to generate the energy sources and the vehicles are not considered. This is negligible with respect to the whole-life emissions of a vehicle since the same machine is constantly used in the industry to produce other vehicles or generate H_2.
- The results do not present any uncertainties study since most of the data sources for the emissions did not have them included [4,42,47,50,51]. Furthermore, including uncertainties in the design spaces of this study would only lead to the misunderstanding of the results.

5. Results and discussion

In this section, the results obtained after applying the methodology and combining the LCA data with the space design results is shown. First, the design spaces were shown as a function of the H_2 mass in the tank, and the GHG-100 and NO_X emissions produced during the manufacturing cycle for each design (Fig. 6) to provide an idea about the considered designs and the implication of such designs in the manufacturing cycle emissions (Section 5.1). Then, GHG-100 emissions produced in the fuel production cycle and in the cradle-to-grave process by each design were analyzed for 500, 600, and 700 km of range FCREx considering SMR with CCS as the H_2 production pathway. This analysis was repeated for a 600 km of range FCREx considering different H_2 production pathways: electrolysis with electricity from the EU mix, SMR and SMR with CCS (Section 5.1.1). The same results were also extracted and discussed for NO_X emissions (Section 5.1.2).

As explained in Section 3.1.3, the design spaces were generated as a function of the battery capacity, the FC maximum power output, and the H_2 tank capacity. All the maps representing the design spaces in this section were shown as a function of the battery capacity (Y axis) and the FC maximum power output (X axis). The H_2 tank capacity was fixed to achieve a target range (500, 600 or 700 km) depending on the design space that is shown.

5.1. Design spaces description and energy carriers lifetime consumption

In this section, the design spaces in terms of H_2 tank capacity, H_2 and total energy consumed along the life as a function of the battery capacity and the FC stack maximum power output are shown in Fig. 6 for FCREx designs with a range of 600, 500 and 700 km. These design spaces are explained so that the tendencies of how the H_2 tank capacity and consumption change with the design and the target range. Then, GHG-100 and NO_X emissions in the manufacturing cycle for these design spaces are shown in Fig. 7 and discussed. This section is intended to provide a detailed explanation of the energy consumption characteristics of each design and how they change when the sizing of the main components under study is modified.

Different powertrain component sizing has a significant effect on both the performance of the vehicle in terms of consumption and range and on the emissions produced in the cradle-to-grave process. Among the impacts the powertrain design has on emissions, it is possible to differentiate two effects. First, there is a direct effect on the emissions produced during the manufacturing of the vehicle. Second, an indirect effect due to the fact that a different powertrain design may affect significantly the H_2 or electricity consumption of the vehicle, thus requiring a lower or higher amount of energy during the whole vehicle life. As such, the second effect only increases the emissions coming from the fuel production cycle, since using H_2 or electricity from batteries to drive a vehicle does not produce any GHG-100 or NO_X emissions during the operation cycle. Nevertheless, in the case of FCREx, there is a third effect coming from the complexity and versatility of the powertrain since it is composed of two power sources: a battery and an FC system. The third effect is also indirect and affects significantly the fuel production cycle since, in this case, there are two types of *fuels* (H_2 and electricity) and the total percentage of H_2 or electricity utilization along the whole life depends on the proportion of energy in the vehicle stored in the tank or in the battery. Therefore, the fuel production cycle could also be affected by the relative amount of *fuel* produced as H_2 or as electricity since the emissions generated in the H_2 production pathway could be significantly larger than those emitted to produce electricity.

Fig. 6 shows in the first row (graphs A–C) how the H_2 tank capacity was modified according to the battery capacity and the FC maximum power output to achieve the target range (calculated using the WLTC 3b driving cycle). In the second row (graphs D–F) the amount of H_2 consumed along the 120,000 km of life is shown while in the third row (graphs G–I) shows the total energy consumed along the whole life, including both H_2 in the tank and the electricity in the battery. All these results were calculated from previous studies [7].

FCREx design and performance change significantly depending on the range (Fig. 6). In the case of the design, it was calculated that the maximum range for FCREx could be around 700 km, given the significant weight of this vehicle that includes two combined powertrains. Nonetheless, with the minimum battery capacity that was considered (30 kWh) it would be possible for these vehicles to achieve a range of 500 km with 3.6–4 kg of H_2 and a range of 600 km with 4.5–4.9 kg of H_2. The range of 700 km would only be achievable with a battery capacity ≥50 kWh, an FC maximum power output >30 kW and approximately 5 kg of H_2. As the H_2 tank increase with the target range, given a fixed battery capacity and FC maximum power, the overall vehicle weight increases without increasing the efficiency of the systems, hence both H_2 and total energy consumption increase with target range (Fig. 6, D–I). As such, it is important to note that depending on the application and the target range for which the vehicle is designed, the energy and H_2 consumption may be affected. This is critical and must be taken into account by FCV designers and manufacturers since, unlike conventional vehicles, changing the tank capacity of an FCREx vehicle may have a significant impact on consumption.

As the battery capacity increases in the FCREx architecture, the H_2 tank capacity decreases since the fraction of the range that can be

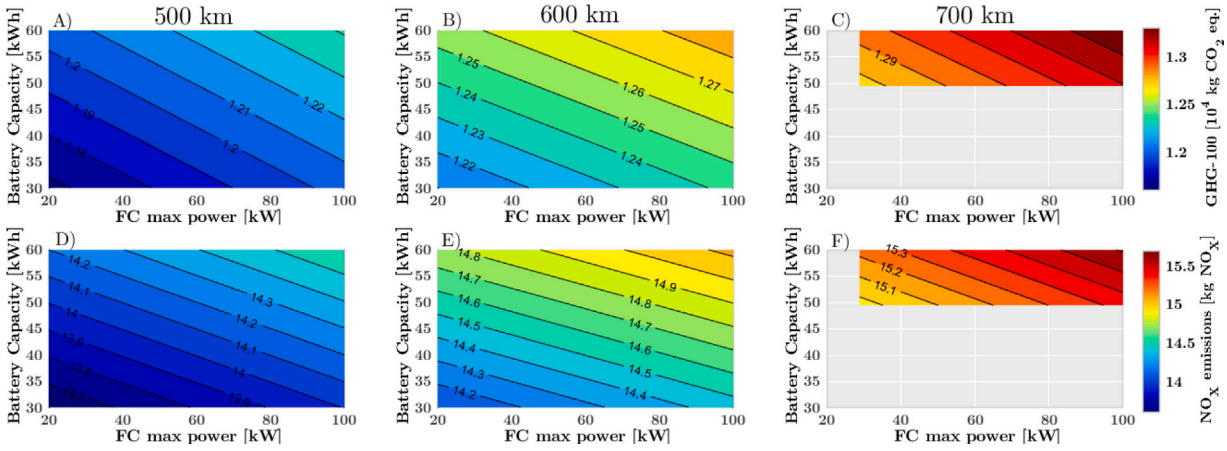

Fig. 7. Design spaces for 500, 600, and 700 km of range FCREx: GHG-100 emissions in the manufacturing cycle (1st row), and NO_X in the manufacturing cycle (2nd row). Functional unit is 1 vehicle. Life is set to 120,000 km.

covered with the battery alone increases, thus allowing the decrease in the H_2 mass for a fixed range (Fig. 6, A–C). As a consequence, the required amount of H_2 to cover 120,000 km also decreases with increasing battery capacity (Fig. 6, D–F). Furthermore, the higher the share of energy produced from the battery increases the overall system efficiency, given the higher efficiency of the battery compared to that of the FC system. Therefore, the overall vehicle efficiency increase despite the higher vehicle weight, thus decreasing the total energy consumed to cover 120,000 km as the battery capacity increases (Fig. 6, G–I). It is important to note here that the decrease in the H_2 consumed is not due to an increase in the FC system efficiency. In fact, the higher vehicle weight implies higher brake power demand along the driving cycle, meaning that the FC system would operate at higher current densities, thus decreasing the efficiency. Rather, the decrease in H_2 comes from the lowest requirement of H_2 to cover a certain range, since the distance that can be covered only with the battery increases.

The main effect of increasing the FC maximum power was to increase the FC system efficiency since, for the same power demand, a higher-power FC stack operates with lower current density, thus decreasing the electrochemical losses associated with the FC stack operation and the BoP power consumption. This implies that H_2 consumption decreases with increasing FC maximum power despite the increase in vehicle weight, hence decreasing the required H_2 tank capacity (Fig. 6, A–C), the H_2 and total energy consumed along the lifetime (Fig. 6, D–I). Differently from what was explained in the previous paragraph, the trend of decreasing H_2 consumption, in this case, is motivated by an increase in the FC system efficiency along the driving cycle. When increasing the FC stack maximum power the range that can be covered using the battery alone is slightly reduced, given the increase in the vehicle weight. Nonetheless, this seems to be compensated by the increase in the FC system efficiency.

It is important to note that, while the iso-H_2-consumed lines are parallel between graphs with different target range (Fig. 6, D–F), in the case of the total energy consumption these lines do not present the same slope between graphs (G–I). This happens because as the target range, the amount of required H_2 increases, thus increasing the fraction of energy stored as H_2. If the fraction of the total energy as H_2 increases, the vehicle efficiency and overall consumption would be more sensitive to increases in efficiency produced over the FC system. This explains why the iso-lines in graphs G–I in Fig. 6 become more vertical as the target range increases, implying higher sensitivity to the FC maximum power output compared to the battery capacity. Therefore, for high-range FCREx, it would be more beneficial in terms of overall energy consumption to target high-power FC stack designs.

From these results, the optimum design of FCREx passenger vehicles in terms of consumption and performance was found to have high battery capacity and high FC stack maximum power. This result suggests that, only in terms of performance, the FCREx nor the conventional FCV architectures are optimum, but a compromise between these two must be achieved. However, the results of this study also indicate that the optimum design in terms of performance may not be implementable into passenger vehicles due to available space and TCO reasons. In contrast, cradle-to-grave emissions may be optimum with the optimum-performance design depending on the H_2 production pathway and the vehicle manufacturing process emissions.

As commented before, the first effect of FCREx design on emissions is derived from the increase in emissions coming from the vehicle manufacturing cycle. This is shown in Fig. 7 in terms of GHG-100 (A–C) and NO_X emissions (D–F). When comparing designs with the same battery capacity and FC maximum power output but different range, those with higher range imply higher GHG-100 and NO_X emissions since the H_2 tank capacity increases, thus producing more emissions during its manufacturing process. However, the relative increase of GHG-100 emissions with target range is more significant compared to NO_X because GHG-100 emissions in the manufacturing process of H_2 tanks scale more with its capacity than NO_X. Both increasing the battery capacity and the FC maximum power imply higher emissions since the increase in emissions produced when manufacturing higher-capacity batteries and higher-power FC stacks outweighs the decrease in emissions due to the decrease in the required H_2 tank capacity shown in Fig. 6, graphs A–C. Note how the emissions shown in Fig. 7 are significantly high compared to those produced in the manufacturing cycle of any fossil-fueled conventional ICE vehicle since the emissions coming from the battery, the FC system, and the H_2 tanks are large compared to the emission required to produce an ICE vehicle. This difference is expected to decrease with time as the H_2-based technologies become more mature and the industry producing them is more developed, thus reducing the costs and emissions due to economies of scale. Nevertheless, the manufacturing cycle is just one part of the cradle-to-grave process, hence the fuel production cycle should also be accounted for (the emissions during the operation cycle are almost negligible and are only GHG-100).

5.1.1. Global warming emissions

In this section, the design spaces were expressed as a function of GHG-100 emissions for the fuel production cycle and the cradle-to-grave process. First, the design spaces for the FCREx vehicles with a target range of 600 km were plotted considering different H_2 production pathways (Fig. 8): electrolysis with the current EU electricity mix, and SMR with and without CCS. With these data, how the emissions vary for a fixed design space when changing the H_2 production pathway is discussed. Then, the design spaces for FCREx with a range of 500, 600 and 700 km for the fuel cycle and the cradle-to-grave associated

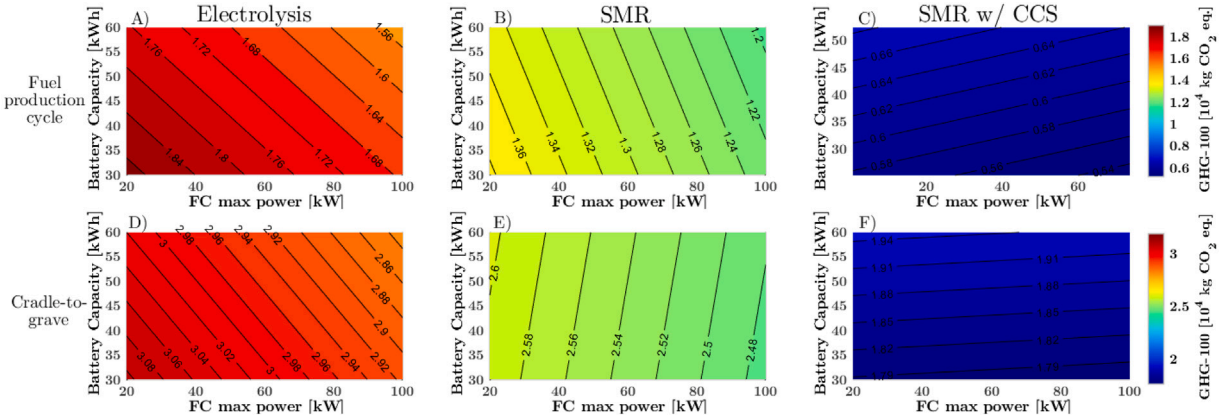

Fig. 8. Design spaces for 600 km of range FCREx: GHG-100 emissions produced in the fuel production cycle and in the cradle-to-grave cycle considering different H_2 production pathways. Functional unit is 120,000 km.

emissions were shown in Fig. 9 considering blue H_2 (H_2 produced through SMR with CCS) since most of the H_2 produced currently is based on SMR technology which can be improved in the short-term with CCS, thus being a more realistic option to reduce emissions in the short-term than green H_2 (produced solely from renewable sources).

The greatest variation of GHG-100 emissions in the graphs of Fig. 8 is produced when changing the H_2 production pathway. This variation in emissions is significantly higher than that produced by varying the design in terms of battery capacity or FC maximum power output, hence the change in emissions produced during the fuel production cycle per kg of H_2 or per kWh of electricity when changing the H_2 production pathway is far more relevant than the decrease in H_2 or electricity consumption as a consequence of changing the powerplant design. Overall, GHG-100 emissions produced in the fuel production cycle increase by ~184 % and ~111 % compared to the production pathway of SMR with CCS for electrolysis with the EU electricity mix and SMR respectively. Analogously, the overall increase in GHG-100 emissions in the cradle-to-grave process with the H_2 production pathway is ~60 % and ~36 % compared to SMR with CCS for electrolysis and SMR respectively. The large relative increase in emissions in the fuel production pathway and the significant increase in the cradle-to-grave process confirm how the fuel production pathway has a great influence on the total emissions. Comparing the overall GHG-100 emissions in the fuel production cycle against the total emissions they could imply around ~33 % in the case of SMR with CCS, ~51 % in the case of SMR, and ~58 % in the case of electrolysis. According to this data, it is possible to conclude that the emissions produced during the manufacturing cycle are always a significant part of those produced in the FCREx cradle-to-grave process and could be more than 50% of the total GHG-100 emissions if low-emissions production pathways such as SMR with CCS are considered. Therefore, the vehicle design would have a higher influence on total emissions if H_2 production pathways imply high emissions (SMR and electrolysis with the EU mix) since the emissions in the fuel production cycle are sensitive to the vehicle efficiency through fuel and electricity consumption (Fig. 6). This means that in a scenario with blue or green H_2 the focus to minimize cradle-to-grave emissions for FCV and FCREx should mostly shift towards the vehicle manufacturing cycle.

The slope of the iso-lines in Fig. 8 represent the sensitivity of the GHG-100 emissions produced in the fuel cycle or in the cradle-to-grave process to the FCREx design. The slope changes significantly with the H_2 production pathway since there are two energy carriers in the vehicle (electricity in the battery and H_2 in the tank) with different emissions per kWh of energy. As such, how GHG-100 emissions change with the FCREx design would depend on which energy carrier implies more emissions per useful,[1] kWh of energy carrier produced. In the case of H_2 produced through electrolysis or SMR (Fig. 8: A,B,D & E), the production of 1 kWh_{useful} of H_2 generates more emissions than 1 kWh_{useful} of electricity due to both the higher efficiency of batteries and the lower emissions per actual kWh. Therefore, in this case, as the battery capacity increases, GHG-100 emissions in the fuel production cycle decrease (A–B). In Fig. 8 the slope of graph A's iso-lines is similar to the slope of the iso-lines in the graph showing the total H_2 consumption along the life (Fig. 6, graph E) since the emissions produced when generating H_2 through electrolysis with the EU electricity mix dominate the overall emissions in the fuel cycle. In contrast, the iso-lines of Fig. 8 graph B are similar to those in Fig. 6 graph H which represents the total energy consumption since producing 1 kWh_{useful} of H_2 generates similar but higher emissions than producing 1 kWh_{useful} of electricity for the battery. The trends of GHG-100 emissions when comparing graphs A and D (electrolysis, Fig. 8) are similar, hence the fuel production cycle dominates most of the cradle-to-grave process. In the case of SMR (graphs B and E) the trends change: increasing the battery capacity increases global emissions despite decreasing both the H_2 and the electricity consumed along the life. This means that if SMR is considered, GHG-100 decrease in such a way that the vehicle manufacturing cycle dominates the cradle-to-grave emissions when the battery capacity increases. Nevertheless, with both electrolysis and SMR as production pathways, cradle-to-grave emissions still decrease with FC maximum power since the efficiency of the FC system increases and most of the energy is stored as H_2. Therefore, the fuel production cycle dominates the global GHG-100 when the FC maximum power changes.

Interestingly, if high-emissions production pathways for H_2 are considered, the optimum FCREx design in terms of cradle-to-grave emissions is found to be the same as that minimizing the H_2 and energy consumption (high battery capacity and high FC stack maximum power) since in this case, the fuel production cycle dominates the overall emissions (Fig. 8, graphs A & D). Hence, minimizing H_2 consumption also means minimizing cradle-to-grave emissions. This trend is also found for NO_X emissions in the following section (Fig. 10, graphs A & D).

The trends found for SMR with CCS in the fuel production cycle are significantly different from those of the other production pathways. In the fuel production cycle (Fig. 8, graph C), the GHG-100 generated per kWh_{useful} of H_2 are much lower than those per kWh_{useful} of electricity, thus increasing the fuel cycle emissions as the battery capacity increases (amount of energy stored as electricity in the vehicle). With all the

[1] Useful kWh means the energy stored as electricity or H_2 multiplied by the mean efficiency of the corresponding system (battery or FC system).

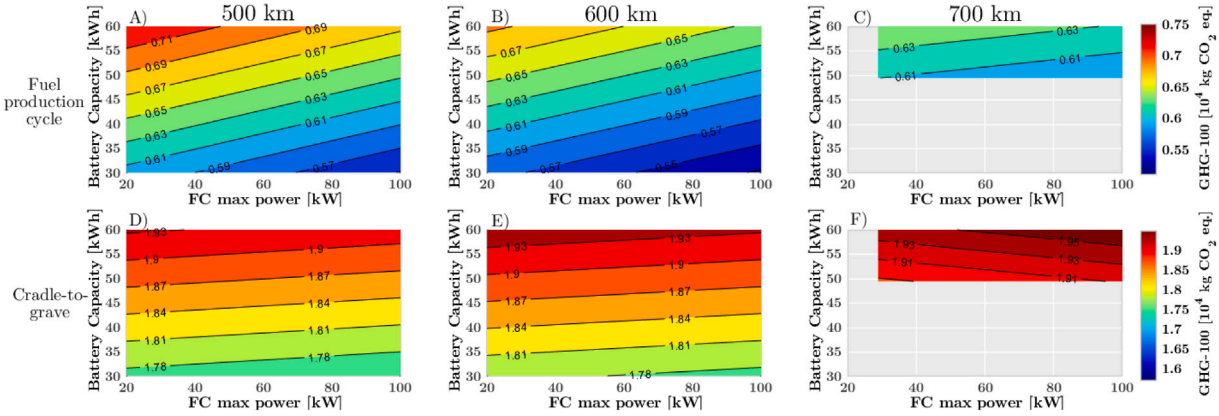

Fig. 9. Design spaces for 500, 600, and 700 km of range FCREx: GHG-100 emissions produced in the fuel production cycle and in the cradle-to-grave cycle considering SMR with CCS as H_2 production pathway. Functional unit is 120,000 km.

production pathways considered, since most of the energy stored is in form of H_2, increasing the FC maximum power clearly decreases the emissions in the fuel production cycle, being SMR with CCS no exception (Fig. 8 graph F). Again, the increase of battery capacity imply higher cradle-to-grave emissions. In the case of considering SMR with CCS, the overall GHG-100 emissions are far more sensitive to battery capacity than SMR without CCS. This is due to the fact that both in the fuel cycle and the cradle-to-grave process GHG-100 emissions increase with battery capacity (both dominate the trend). This is indicative of the consequences of using low-emission fuels such as blue or green H_2 to power FCV. First, the aim to reduce emissions shifts towards the vehicle manufacturing cycle since it dominates the cradle-to-grave emissions. Second, using electricity from batteries if the renewable share in the electricity mix does not improve may only increase the cradle-to-grave emissions.

Fig. 9 shows the fuel production cycle and the cradle-to-grave emissions for different target range FCREx with H_2 produced through SMR with CCS. Note again how the GHG-100 emissions of blue H_2 are lower than those of electricity. The graphs A–C are analogous to graph C in Fig. 8, showing how GHG-100 emissions increase with the battery capacity and decrease with the FC maximum power due to the low emissions produced in the SMR with CCS process. In these graphs, it is possible to see how the GHG-100 emissions in the fuel production cycle decrease with the target range for a fixed design. Interestingly this happens because, for a given battery capacity, as the target range increases, the amount of H_2 stored increases, thus increasing the percentage of the whole life (distance) that is covered using only H_2. If GHG-100 emissions per kWh_{useful} of H_2 were higher than those produced per kWh_{useful} of electricity (SMR or electrolysis) in the fuel production cycle, then the overall GHG-100 in the fuel cycle would increase with the target range.

In the case of cradle-to-grave GHG-100 emissions, increasing the range for a fixed combination of battery capacity and FC stack maximum output power increases GHG-100 emissions (Fig. 9 graphs D–F). This happens because the decrease in emissions in the fuel cycle (Fig. 9 graphs A–C) is lower than the increase in the manufacturing cycle emissions due to the need for bigger H_2 tanks (Fig. 7 graphs A–C) when increasing the target range. When the target range is kept constant at 500 or 600 km, graphs D–E show how GHG-100 emissions increase with battery capacity and decrease with FC maximum power, as explained for Fig. 8, graph F. In contrast, for the design space with a target range of 700 km the emissions trend with respect to the FC maximum power changes, implying an increase in GHG-100 with this sizing parameter. The change in trend is motivated by the high weight of the FCREx with such target range, which limits the decrease in H_2 consumption (Fig. 6, graph F) with the FC maximum power, making the increase in emissions in the manufacturing cycle outweigh the decrease in the fuel cycle.

From the data in Fig. 9 cradle-to-grave GHG-100 emissions may vary up to 10% depending on the components sizing and the target range FCREx are designed for. This value may seem small, but actually it is significant if it is considered that the comparison is performed between vehicles that use the same power sources (H_2 and electricity) with constant production pathway and similar architecture, albeit the sizing of the components may vary.

In conclusion, the use of FCREx provides significant variability in GHG-100 emissions with the design, the target range and the H_2 production pathway. Therefore, these emissions must be taken into account in the vehicle development process. With low-emission H_2 production strategies, decreasing the FCREx target range and decreasing the battery size could reduce emissions since the vehicle manufacturing cycle becomes the dominant phase in the cradle-to-grave process. As such, depending on how the H_2 production infrastructure evolves in the following decades, the optimum FCREx in terms of GHG-100 emissions may evolve towards moderate-to-high FC stack power and moderate-to-low battery capacities. This optimum design may imply lower-than-BEV manufacturing costs and low but not minimum H_2 and total energy consumption (Fig. 6) [7]. This optimum might be in line with the optimum design in terms of TCO.

5.1.2. NO_X emissions

NO_X emissions are also analyzed in this study since they are a major concern for society due to the harmful effects of these gases on human health and ozone generation/depletion. This section follows the same structure as Section 5.1.1 but focused on NO_X emissions. Note that, differently from GHG-100, the SMR production pathway produces the least NO_X emissions (Fig. 10) since SMR with CCS requires additional resources and energy to capture the CO_2 and the EU electricity mix is not renewable-enough to produce low-NO_X H_2 from electrolysis. As a consequence, compared to the H_2 production pathway SMR with CCS, overall NO_X emissions change in the fuel cycle by ~95% and ~ −16% considering electrolysis and SMR without CCS, respectively. Analogously, in the cradle-to-grave process overall NO_X emissions change by ~38% and ~ −6%. From the overall change in emissions with the production pathway, it is possible to identify that their influence is significant by much lower than for GHG-100 emissions. Given the relatively small variation in NO_X emissions and the large difference in GHG-100 emissions between SMR with and without CCS, it could be favorable to consider SMR with CCS as the optimum production pathways to reduce overall emissions (among those considered in this study).

Producing H_2 from electrolysis implies much higher NO_X emissions since a significant part of the electricity mix is produced from fossil fuels. In the SMR process, the NO_X are produced in the combustion of the fuel used to heat the reactor. In this case, low-NO_X burners and

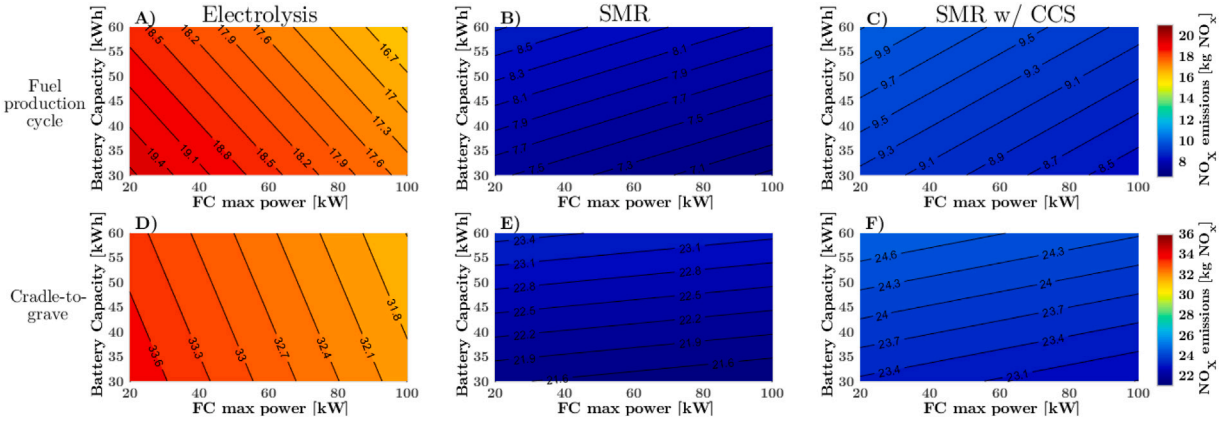

Fig. 10. Design spaces for 600 km of range FCREx: NO_X emissions produced in the fuel production cycle and in the cradle-to-grave cycle considering different H_2 production pathways. Functional unit is 120,000 km.

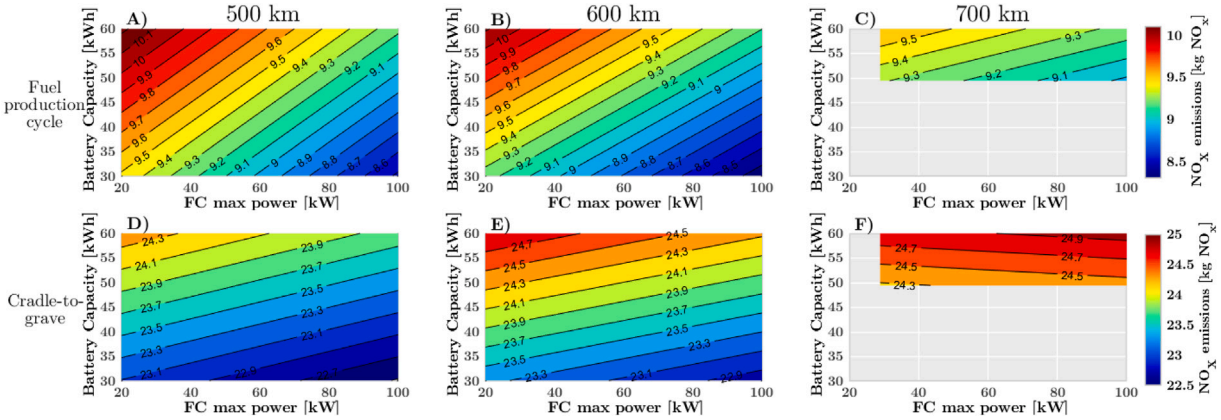

Fig. 11. Design spaces for 500, 600, and 700 km of range FCREx: NO_X emissions produced in the fuel production cycle and in the cradle-to-grave cycle considering SMR with CCS as H_2 production pathway. Functional unit is 120,000 km.

selective catalyst reduction (SCR) exhaust gas after treatments are a feasible option to minimize NO_X in SMR plants, although their use is not widely extended [52].

When H_2 is produced from electrolysis (Fig. 10, graphs A & D), NO_X emissions decrease when increasing the FC maximum power output and the battery capacity, both in the fuel cycle (graph A) and in the cradle-to-grave process (graph D). As explained before, the evolution of NO_X emissions in the fuel cycle is justified by the decrease in energy and H_2 consumption. The emissions produced in the H_2 production cycle seem to be high than that produced to generate the electricity for the battery. As a consequence, the decrease in emissions when raising the FC maximum power is more significant than when increasing the battery capacity. The trends of the fuel cycle and the cradle-to-grave process opposed to that found in the manufacturing cycle (Fig. 7, graph E), where NO_X emissions increase with the FC power and the battery capacity. This means that the evolution of cradle-to-grave emissions is dominated by the fuel cycle. In this case, the fuel cycle also produces more emissions than the manufacturing cycle (16.4–19.7 kg NO_X against 14.1–15.1 kg NO_X), implying that the fuel production strategy dominates the global emissions both in trend and amount.

NO_X emissions evolution and the amount produced are very similar in the cases of producing the H_2 from SMR with or without CCS (Fig. 10, graphs B, C, E & D). In the fuel cycle (graphs B & C), NO_X emissions decrease with the FC stack maximum power due to the lower H_2 consumption. In contrast, they increase with the battery capacity since producing electricity produces more emissions than producing H_2. In this sense, the fraction of energy stored as H_2 decreases, thus increasing the electricity usage to achieve a certain range. Regarding the cradle-to-grave emissions, they show the same evolution with respect to design parameters as the fuel cycle, hence they are dominated by the fuel cycle emissions. Nonetheless, the emissions in the fuel cycle are significantly lower than those in the manufacturing cycle, which means that although the manufacturing cycle is responsible for most of NO_X emissions, the sensitivity of the fuel cycle to the FCREx design is higher, thus dominating the trends but not the total emissions.

Complementary to Figs. 10, 11 shows the NO_X emissions in the fuel cycle and the cradle-to-grave process for designs with 500, 600 and 700 km of range considering blue H_2 (SMR with CCS). The evolution of NO_X emissions in the graphs A–C is analogous to that in Fig. 10 graph C and it is explained in the previous paragraph. For a given design, in terms of battery capacity and FC maximum power, increasing the range implies lower NO_X emissions in the fuel cycle since more H_2 is required to increase the range and the emissions of blue H_2 are lower than those produced to generate electricity with the EU mix. This trend in the fuel cycle is the same found for GHG-100 emissions in Fig. 9. In the design space of 700 km, NO_X emissions are less sensitive to the variation of the FC maximum power because the gain in efficiency when increasing the FC power is less significant due to the high vehicle weight. This can also be appreciated in the total H_2 consumption calculated for this design space (Fig. 6, graph F).

Graphs D–F of Fig. 11 show how cradle-to-grave NO_X emissions, for a given combination of battery capacity and FC maximum power, increase with target range due to the additional emissions coming from requiring higher-capacity H_2 tanks. Furthermore, the change in NO_X trend when comparing graphs D–E with graph F results from the decrease of the sensitivity of the emissions produced in the fuel cycle

with the FC maximum power, thus allowing the vehicle manufacturing cycle dominates the tendency. As such, in the design space of 700 km, NO_X emissions increase with the FC maximum power.

The variation between worst and best designs in terms of cradle-to-grave NO_X emissions can be up to 10% within the generated design spaces. This variation is similar to that found for GHG-100 emissions, which is a consequence of the same trend they follow when changing the sizing of the components.

To conclude, differently from GHG-100 emissions, NO_X emissions for FCREx seem to be mostly dominated by the fuel production process, except for the designs with a high target range (700 km) where the weight becomes an obstacle to decrease significantly H_2 consumption by increasing the FC maximum power. As such, the designs offering the lowest NO_X emissions in the cradle to grave process are those with a battery of 30 kWh and high Fc maximum power, except for the design space of 700 km. The production pathway that offered the lowest NO_X was SMR without CCS since CCS process requires an extra amount of energy to enable CO_2 capture. Nevertheless, the difference between SMR with and without CCS in NO_X is substantially smaller than that found for GHG-100. Therefore, looking at overall emissions, SMR with CCS may still be the optimum H_2 production pathway among those considered in this study.

5.2. Potential of cradle-to-grave emissions decrease with FCREx architecture

From the results shown along this section, it was concluded that with low-emissions H_2 production pathways (blue H_2), the design trend to minimize cradle-to-grave emissions of FCREx vehicles should focus on decreasing the battery capacity to the minimum possible to ensure enough range in BEV mode so that the emissions produced during the manufacturing of the batteries are minimum and high FC stack maximum power to decrease H_2 consumption. In other words, this trend suggests that the FCREx architecture could produce higher cradle-to-grave GHG-100 and NO_X emissions than conventional FCV architectures.

In contrast, with high-emissions H_2 production pathways (electrolysis from the current EU electricity mix), the FCREx architecture could decrease significantly the GHG-100 and NO_X emissions with higher battery capacities (Figs. 8 and 10, graph D). This suggests that the interest in FCREx architecture, only regarding cradle-to-grave emissions, would depend on the balance between the emissions produced when generating electricity and those released when producing H_2. However, there is another factor that would affect significantly the cradle-to-grave emission of FCREx architecture: the emissions produced in the battery manufacturing process. Therefore, it is possible to deduce that, in the short term, if H_2 is produced from the EU electricity mix, FCREx would have significant advantages over FCV in terms of emissions. In the medium and long-term it is uncertain whether FCREx or conventional FC architectures will produce lower emissions since it will depend on the rate at which the EU electricity mix, the H_2 production pathways, and the battery production process are decarbonized and become cleaner. The results derived from this study will serve the FCV manufacturers to understand the performance and cradle-to-grave emissions of FCREx vehicles and their variation with the design choice regarding changes in FC stack maximum power, battery capacity and H_2 tank capacity. This could also serve as a starting point for the design process of FCV vehicles with FCREx architecture to down-select a set of design choices to be further refined as the vehicle development advances. The relevance of producing such results not only lies in the benefits for FCV manufacturers but rather for society in general since the existence of these design spaces both in terms of performance and emissions could shorten significantly the FCREx vehicle process, thus accelerating the path towards the H_2 economy and decreasing the environmental impact of the transport sector.

Finally, from this analysis, a set of recommendations to decrease the cradle-to-grave emissions of FCREx vehicles could be extracted. First, it is imperative to invest in decarbonizing and decreasing the overall emissions of the vehicle manufacturing process, especially battery manufacturing, since it is responsible for a significant part of the cradle-to-grave emissions. Second, the renewable share on the EU electricity mix should increase since it will have a direct impact on both electricity and H_2 production. Third, in other to drastically decrease the cradle-to-grave emissions of FCV in general, it is necessary to implement CCS technology in SMR plants, since this process would allow increasing the renewable share of the EU electricity mix at a faster rate in parallel to decarbonizing the H_2 production pathway which will imply a higher rate of decrease of global emissions rather than dedicating all the renewable energy infrastructure into producing green H_2. Fourth, due to the uncertainty on the cradle-to-grave emissions of FCREx caused by its use of different energy sources and powerplants, this kind of LCA analysis should be revised over time to adapt these recommendations since important changes are expected in the emissions produced in the battery manufacturing process, the EU electricity mix [53], and the H_2 production pathways.

6. Conclusions

In this study, the design spaces, H_2, energy lifetime consumption, GHG-100 and NO_X emissions were analyzed by combining sizing with life cycle assessment (LCA) methodologies. The only impact category considered was greenhouse gases (GHG-100) since they are the emissions of the utmost scientific and social concern, although NO_X were also estimated. The design spaces, calculated in previous studies, were expressed as a function of the battery capacity, the FC stack maximum power output at the limiting current density and the H_2 tank capacity. These three design parameters were related through 1D simulations of the fuel cell range-extender (FCREx) complete architecture in WLTC 3b driving cycle for the selected ranges of 500, 600 and 700 km. Furthermore, for the design space with 600 km of range, electrolysis with electricity from the current EU mix, steam methane reforming (SMR) with and without carbon capture and storage (CCS) were considered as the H_2 production pathways to understand the cradle-to-grave emissions of these vehicles on different feasible-in-the-short-term H_2 production scenarios. Green H_2 from only renewable sources was not considered since it is not a feasible solution in the short-term and considering it would only lead to misinterpreting the actual emissions of these vehicles for the following 5–15 years.

The design spaces, the H_2, and energy consumption along the lifetime were calculated, from which it was concluded that both increasing the battery capacity and the FC stack maximum power decreased the H_2 and energy consumption, hence decreasing the emissions in the fuel cycle and increasing those in the vehicle manufacturing cycle. This happened since increasing the battery capacity leads to a decrease in the H_2 capacity, thus implying that a greater part of the lifetime should be covered with the battery alone, which is more efficient than the FCREx mode despite the higher weight. Furthermore, it was found that increasing the FC maximum stack power decreased the H_2 consumption since the FC stack operated at lower current densities, thus increasing the FC system efficiency despite the vehicle weight increase. These results were directly used as inputs in the LCA analysis to estimate the vehicle manufacturing and fuel production cycle associated emissions.

In the cradle-to-grave process, GHG-100 emissions increase by ~60% and ~36% with electrolysis and SMR without CCS compared to SMR with CCS or blue H_2. Analogously, NO_X emissions change by ~38% and ~ −6%. The decrease in NO_X emissions with SMR without CCS was justified with the extra energy and resources required to enable CCS. These data showed how sensitive the overall GHG-100 and NO_X emissions are with the H_2 production pathway. For both GHG-100 and NO_X emissions, the vehicle manufacturing cycle produced most of the cradle-to-grave process, although not always this cycle dominated

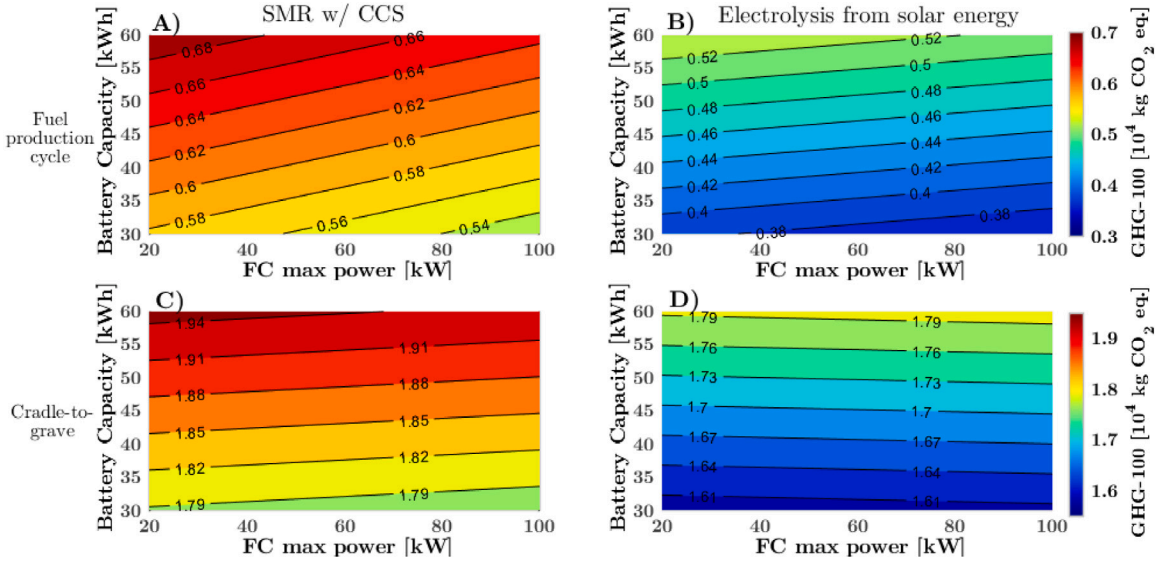

Fig. A.12. Design spaces for 600 km of range FCREx: GHG-100 emissions produced in the fuel production cycle and in the cradle-to-grave cycle considering blue (1st column) and green (2nd column) H_2. Functional unit is 120,000 km.

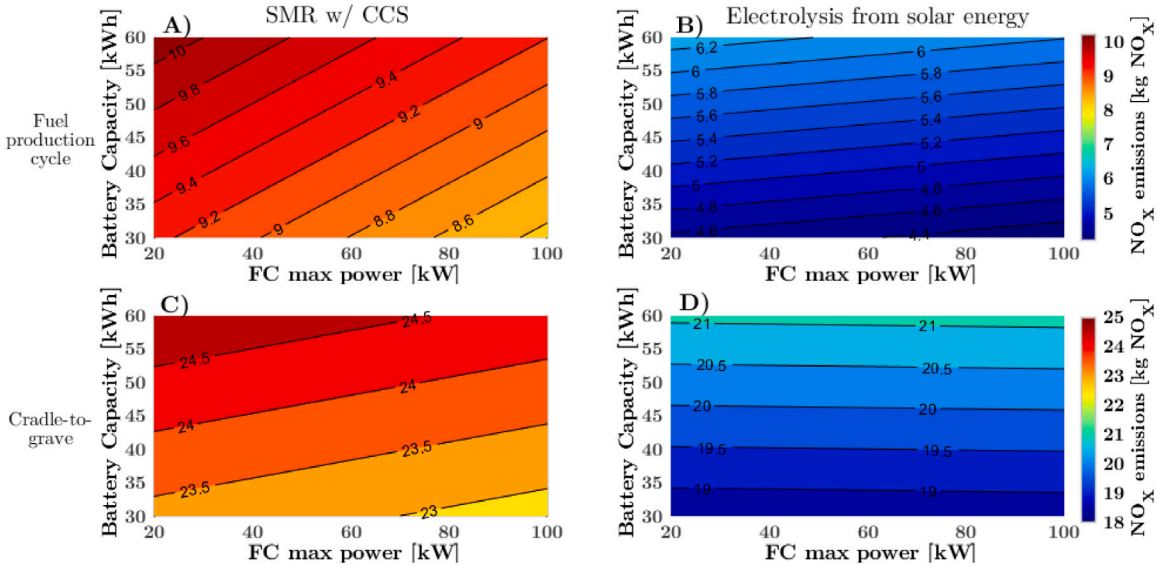

Fig. A.13. Design spaces for 600 km of range FCREx: NO_X emissions produced in the fuel production cycle and in the cradle-to-grave cycle considering blue (1st column) and green (2nd column) H_2. Functional unit is 120,000 km.

how the overall emissions change with the design. With the SMR with CCS as the production pathway, the manufacturing cycle dominated together with the fuel cycle the sensitivity of the cradle-to-grave process when the battery capacity increased but the trend in emissions when the FC maximum power increase was clearly dominated by the fuel cycle, except for NO_X emissions in the FCREx designs with 700 km of range. Both cradle-to-grave GHG-100 and NO_X emissions may vary up to 10% when comparing the worst and best design among those considered.

With blue H_2, increasing the battery capacity increased NO_X as well as GHG-100 emissions in both the fuel production and vehicle manufacturing cycles, despite decreasing the energy consumption, since the emissions produced in this pathway are smaller compared to those produced to generate electricity. This means that, in order to minimize overall emissions, FCREx should be designed with moderate-to-low battery capacities. Interestingly, it was found that for most of the design spaces, increasing the FC maximum power decreased overall cradle-to-grave GHG-100 and NO_X emissions, as well as overall H_2 consumed along the lifetime. Therefore, in terms of overall emissions and with low but not minimum H_2/energy consumption, the optimum FCREx design should have a moderate-to-small battery enough to cover a certain range of operation in battery mode only and moderate-to-high FC stack maximum power in contrast to the optimum design in terms of consumption, which was found to have high battery capacity and high FC stack maximum power. Nonetheless, the fact that the performance-wise and the emissions-wise optimum designs coincide or not, depends mainly on the H_2 production pathway and the vehicle manufacturing process. In the case of considering high-emissions H_2 production pathways (electrolysis from EU mix), these optimum designs overlap because minimizing H_2 consumption means minimizing cradle-to-grave emissions. Although small-to-moderate battery size is recommended, there still exists a trade-off in terms of the total cost of ownership (TCO), emissions and consumption that makes FCREx a promising FCV architecture in the short-to-medium term, given the flexible operation it can offer, the high H_2 prices, the lower energy consumption and the low availability of H_2 refueling stations.

Finally, a set of recommendations were suggested to decrease the cradle-to-grave emissions of FCREx vehicles. They were: decarbonizing the battery manufacturing process, decarbonizing the EU electricity mix, prioritizing blue H_2 over green H_2 to maximize the rate of decrease of cradle-to-grave emissions, and refreshing the data of this analysis over time so that the recommendation can be adapted to the scenario in that moment, given the uncertainty on how the manufacturing and fuel production processes will evolve with time.

CRediT authorship contribution statement

J.M. Desantes: Conceptualization, Project administration, Supervision. **R. Novella:** Investigation, Formal analysis, Writing – review & editing. **B. Pla:** Resources, Methodology, Software, Data curation. **M. Lopez-Juarez:** Investigation, Methodology, Validation, Software, Writing – original draft.

Acknowledgment

This research has been partially funded by the Spanish Ministry of Science, Innovation and University through the University Faculty Training (FPU) program (FPU19/00550). Funding for open access charge: CRUE-Universitat Politècnica de València

Appendix. Blue and green H_2 comparison

As a complementary section to this study, in this part the GHG-100 and NO_X emissions of the FCREx architecture design spaces considering blue and green H_2 are compared. The pathway defining green H_2 production was exactly the same as that for black H_2 presented in Fig. 5 but changing the source of the electricity used for the electrolysis process with electricity produced from solar energy. As such, the fuel production cycle emissions of green H_2 are significantly smaller compared to those of any other production pathway (0.056 kg CO_2 eq./kWh H_2 and $6.8{\cdot}10^{-5}$ kg NO_X/kWh H_2). Nevertheless, the results in Figs. A.12 and A.13 must be analyzed carefully to identify the scenario they represent. For green H_2, the source of energy is renewable, while for the electricity in the battery, the source is the electricity mix. Therefore, these results represent and scenario that may lead to a certain bias towards FCV rather than towards BEV since it could be argued that renewable energy could be part of the electricity mix thus decreasing the emissions coming from using the battery. This is the reason why these results were included in the appendix only for completeness and must be analyzed taking into account the particular scenario just described.

It is important to note that green H_2 emissions are not completely zero since some of the processes in the production pathway require the use of non-renewable energy for H_2 treatment and distribution. Nonetheless, the global emissions of the process are still significantly lower than with other H_2 production pathways.

In Fig. A.12 the GHG-100 emissions produced during the fuel cycle and cradle-to-grave process are shown for both blue (left column) and green (right column) H_2 for a 600 km of range FCREx vehicle. This same information is presented for NO_X in Fig. A.13. In these two figures the trends of increasing or decreasing the emissions are the same, hence a common explanation can be given to explain them. For both blue and green H_2 increasing the battery capacity implies an increase in emissions since the GHG-100 and NO_X emissions released when producing 1 kWh of H_2 are significantly lower than those for producing 1 kWh of electricity with the current electricity mix. Therefore, emissions decrease with increasing battery capacity since increasing the battery capacity implies a higher usage of electricity and a lower H_2 tank capacity (Fig. 6). The emissions variation with the FC maximum power is that explained along the study: increasing the FC maximum power implies a more efficient use of H_2, thus requiring less fuel to cover a given distance and thus decreasing emissions.

As explained in Section 5, changing the H_2 production pathway does not only imply a variation on the cradle-to-grave process emissions but also on the relative weight of the fuel production cycle. In the case of blue H_2 the fuel production cycle supposes ~33% of the total emissions while for green H_2 it is ~26%. This is, again, a proof of the fact that as the industry moves towards low emissions propulsion systems and/or fuels, the vehicle manufacturing cycle will become more relevant in the cradle-to-grave emissions.

When comparing how the emissions change in the cradle-to-grave process with blue and green H_2 in both Figs. A.12 and A.13, it is possible to identify how increasing the FC maximum power if green H_2 is considered yields higher emissions. This is justified by the low emissions produced by green H_2 in the fuel production process, whose variation when sizing the components of the FCREx architecture is even smaller than the change in emissions in the vehicle manufacturing cycle. As a consequence, the cradle-to-grave emissions of green H_2 present a similar trend to the emissions in the vehicle manufacturing cycle (Fig. 7, graphs B & E).

Finally, it is important to understand that for green H_2 the GHG-100 and NO_X emissions in the cradle-to-grave process may change up to 11.8% and 12.5% depending on the sizing choice respectively, in contrast with blue H_2 whose GHG-100 and NO_X may vary up to 9.1% and 8.8% respectively. This is motivated by the lower absolute value of total emissions for green H_2, which makes the vehicle manufacturing cycle dominate the cradle-to-grave emissions.

References

[1] Fuel Cells & Hydrogen (FCH). Hydrogen roadmap Europe - a sustainable pathway for the European energy transition. first ed.. Publications Office of the European Union; 2019, p. 70. http://dx.doi.org/10.2843/341510.

[2] Wang J, Wang H, Fan Y. Techno-economic challenges of fuel cell commercialization. Engineering 2018;4(3):352–60. http://dx.doi.org/10.1016/j.eng.2018.05.007.

[3] García A, Monsalve-Serrano J, José Sanchís E, Fogué-Robles A. Exploration of suitable injector configuration for dual-mode dual-fuel engine with diesel and OMEx as high reactivity fuels. Fuel 2020;280(June):118670. http://dx.doi.org/10.1016/j.fuel.2020.118670.

[4] Desantes JM, Molina S, Novella R, Lopez-Juarez M. Comparative global warming impact and NOX emissions of conventional and hydrogen automotive propulsion systems. Energy Convers Manage 2020;221(X):113137. http://dx.doi.org/10.1016/j.enconman.2020.113137.

[5] Gandolfi A, Patel A, Vigna MD, Pombeiro M, Pidoux M. Green hydrogen the next transformational driver of the utilities industry. Tech. rep., Goldman Sachs; 2020.

[6] International Energy Agency. The future of hydrogen. In: The future of hydrogen. Tech. rep., (June). 2019, http://dx.doi.org/10.1787/1e0514c4-en.

[7] Molina S, Novella R, Pla B, Lopez-Juarez M. Optimization and sizing of a fuel cell range extender vehicle for passenger car applications in driving cycle conditions, vol. 285. (January). Elsevier Ltd; 2021.

[8] Purnima P, Jayanti S. Optimal sizing of a fuel processor for auxiliary power applications of a fuel cell-powered passenger car. Int J Hydrogen Energy 2020;45(48):26005–19. http://dx.doi.org/10.1016/j.ijhydene.2020.03.127.

[9] Purnima P, Jayanti S. Fuel processor-battery-fuel cell hybrid drivetrain for extended range operation of passenger vehicles. Int J Hydrogen Energy 2019;44(29):15494–510. http://dx.doi.org/10.1016/j.ijhydene.2019.04.081.

[10] Changizian S, Ahmadi P, Raeesi M, Javani N. Performance optimization of hybrid hydrogen fuel cell-electric vehicles in real driving cycles. Int J Hydrogen Energy 2020;45(60):35180–97. http://dx.doi.org/10.1016/j.ijhydene.2020.01.015.

[11] Feroldi D, Carignano M. Sizing for fuel cell/supercapacitor hybrid vehicles based on stochastic driving cycles. Appl Energy 2016;183:645–58. http://dx.doi.org/10.1016/j.apenergy.2016.09.008.

[12] Xu L, Ouyang M, Li J, Yang F, Lu L, Hua J. Optimal sizing of plug-in fuel cell electric vehicles using models of vehicle performance and system cost. Appl Energy 2013;103:477–87. http://dx.doi.org/10.1016/j.apenergy.2012.10.010.

[13] Xu L, Mueller CD, Li J, Ouyang M, Hu Z. Multi-objective component sizing based on optimal energy management strategy of fuel cell electric vehicles. Appl Energy 2015;157:664–74. http://dx.doi.org/10.1016/j.apenergy.2015.02.017.

[14] Wu Z, Wang C, Wolfram P, Zhang Y, Sun X, Hertwich E. Assessing electric vehicle policy with region-specific carbon footprints. Appl Energy 2019;256(7491):113923. http://dx.doi.org/10.1016/j.apenergy.2019.113923.

[15] Wu X, Hu X, Yin X, Peng Y, Pickert V. Convex programming improved online power management in a range extended fuel cell electric truck. J Power Sources 2020;476(2019):228642. http://dx.doi.org/10.1016/j.jpowsour.2020.228642.

[16] Gaikwad SD, Ghosh PC. Sizing of a fuel cell electric vehicle: A pinch analysis-based approach. Int J Hydrogen Energy 2020;45(15):8985–93. http://dx.doi.org/10.1016/j.ijhydene.2020.01.116.

[17] Hu Z, Li J, Xu L, Song Z, Fang C, Ouyang M, et al. Multi-objective energy management optimization and parameter sizing for proton exchange membrane hybrid fuel cell vehicles. Energy Convers Manage 2016;129:108–21. http://dx.doi.org/10.1016/j.enconman.2016.09.082.

[18] Fan A, Wang J, He Y, Perčić M, Vladimir N, Yang L. Decarbonising inland ship power system: Alternative solution and assessment method. Energy 2021;226(X). http://dx.doi.org/10.1016/j.energy.2021.120266.

[19] Perčić M, Ančić I, Vladimir N. Life-cycle cost assessments of different power system configurations to reduce the carbon footprint in the Croatian short-sea shipping sector. Renew Sustain Energy Rev 2020;131(December 2019). http://dx.doi.org/10.1016/j.rser.2020.110028.

[20] Perčić M, Vladimir N, Fan A. Life-cycle cost assessment of alternative marine fuels to reduce the carbon footprint in short-sea shipping: A case study of Croatia. Appl Energy 2020;279(June). http://dx.doi.org/10.1016/j.apenergy.2020.115848.

[21] García A, Monsalve-Serrano J, Villalta D, Lago Sari R, Gordillo Zavaleta V, Gaillard P. Potential of e-Fischer Tropsch diesel and oxymethyl-ether (OMEx) as fuels for the dual-mode dual-fuel concept. Appl Energy 2019;253(July):113622. http://dx.doi.org/10.1016/j.apenergy.2019.113622.

[22] Fernández-Dacosta C, Shen L, Schakel W, Ramirez A, Kramer GJ. Potential and challenges of low-carbon energy options: Comparative assessment of alternative fuels for the transport sector. Appl Energy 2019;236(May 2018):590–606. http://dx.doi.org/10.1016/j.apenergy.2018.11.055.

[23] Bongartz D, Doré L, Eichler K, Grube T, Heuser B, Hombach LE, et al. Comparison of light-duty transportation fuels produced from renewable hydrogen and green carbon dioxide. Appl Energy 2018;231(September):757–67. http://dx.doi.org/10.1016/j.apenergy.2018.09.106.

[24] Bareiß K, de la Rua C, Möckl M, Hamacher T. Life cycle assessment of hydrogen from proton exchange membrane water electrolysis in future energy systems. Appl Energy 2019;237(July 2018):862–72. http://dx.doi.org/10.1016/j.apenergy.2019.01.001.

[25] Ehrenstein M, Galán-Martín A, Tulus V, Guillén-Gosálbez G. Optimising fuel supply chains within planetary boundaries: A case study of hydrogen for road transport in the UK. Appl Energy 2020;276(June):115486. http://dx.doi.org/10.1016/j.apenergy.2020.115486.

[26] Evangelisti S, Tagliaferri C, Brett DJ, Lettieri P. Life cycle assessment of a polymer electrolyte membrane fuel cell system for passenger vehicles. J Cleaner Prod 2017;142:4339–55. http://dx.doi.org/10.1016/j.jclepro.2016.11.159.

[27] Agostini A, Belmonte N, Masala A, Hu J, Rizzi P, Fichtner M, et al. Role of hydrogen tanks in the life cycle assessment of fuel cell-based auxiliary power units. Appl Energy 2018;215(June 2017):1–12. http://dx.doi.org/10.1016/j.apenergy.2018.01.095.

[28] Navas-Anguita Z, García-Gusano D, Dufour J, Iribarren D. Prospective techno-economic and environmental assessment of a national hydrogen production mix for road transport. Appl Energy 2020;259(August 2019):114121. http://dx.doi.org/10.1016/j.apenergy.2019.114121.

[29] Dimitrova Z, Maréchal F. Environomic design for electric vehicles with an integrated solid oxide fuel cell (SOFC) unit as a range extender. Renew Energy 2017;112:124–42. http://dx.doi.org/10.1016/j.renene.2017.05.031.

[30] Corbo P, Migliardini F, Veneri O. Experimental analysis of a 20 kWe PEM fuel cell system in dynamic conditions representative of automotive applications. Energy Convers Manage 2008;49(10):2688–97. http://dx.doi.org/10.1016/j.enconman.2008.04.001.

[31] Corbo P, Migliardini F, Veneri O. Experimental analysis and management issues of a hydrogen fuel cell system for stationary and mobile application. Energy Convers Manage 2007;48(8):2365–74. http://dx.doi.org/10.1016/j.enconman.2007.03.009.

[32] Teng T, Zhang X, Dong H, Xue Q. A comprehensive review of energy management optimization strategies for fuel cell passenger vehicle. Int J Hydrogen Energy 2020;45(39). http://dx.doi.org/10.1016/j.ijhydene.2019.12.202.

[33] Hyundai. Hyundai nexo - technical specifications. p. 0–2.

[34] Sciarretta A, Guzzella L. Control of hybrid electric vehicles. IEEE Control Syst Mag 2007;27(2):60–70.

[35] Onori S, Serrao L, Rizzoni G. Hybrid electric vehicles: energy management strategies. Springer; 2016.

[36] Luján JM, Guardiola C, Pla B, Reig A. Cost of ownership-efficient hybrid electric vehicle powertrain sizing for multi-scenario driving cycles. Proc Inst Mech Eng D 2016;230(3):382–94.

[37] Serrao L, Onori S, Rizzoni G. ECMS as a realization of Pontryagin's minimum principle for HEV control. In: 2009 American control conference. IEEE; 2009, p. 3964–9.

[38] Howell D, Cunningham B, Duong T, Faguy P. Overview of the DOE VTO advanced battery R&D program. Tech. rep., U.S. Department Of Energy; 2016, p. 24.

[39] Ballard. Product data sheet - FCvelocity-MD. 2016.

[40] Ballard. Product data sheet - FCmove-HD. 2016.

[41] USDepartment Of Energy. DOE Technical targets for onboard hydrogen storage for light-duty vehicles. 2015.

[42] IPCC. Climate change 2014. In: Core Writing Team RP, Meyer L, editors. Synthesis report. contribution of working groups I, II and III to the fifth assessment report of the intergovernmental panel on climate change. Tech. rep., Cambridge: Cambridge University Press; 2015, p. 3–22.

[43] Cheng F, Porter MD, Colosi LM. Is hydrothermal treatment coupled with carbon capture and storage an energy-producing negative emissions technology? Energy Convers Manage 2020;203(August 2019):112252. http://dx.doi.org/10.1016/j.enconman.2019.112252.

[44] Choi W, Song HH. Well-to-wheel greenhouse gas emissions of battery electric vehicles in countries dependent on the import of fuels through maritime transportation: A South Korean case study. Appl Energy 2018;230(August):135–47. http://dx.doi.org/10.1016/j.apenergy.2018.08.092.

[45] Obnamia JA, Dias GM, MacLean HL, Saville BA. Comparison of U.S. Midwest corn stover ethanol greenhouse gas emissions from GREET and GHGenius. Appl Energy 2019;235(October 2018):591–601. http://dx.doi.org/10.1016/j.apenergy.2018.10.091.

[46] Al-Qahtani A, Parkinson B, Hellgardt K, Shah N, Guillen-Gosalbez G. Uncovering the true cost of hydrogen production routes using life cycle monetisation. Appl Energy 2021;281:115958. http://dx.doi.org/10.1016/j.apenergy.2020.115958.

[47] European Environmental Agency (EEA). Overview of electricity production and use in Europe - Indicator Assessment. 2018.

[48] Council of European Energy Regulators (CEER). CEER report on power losses. Tech. rep., 2017.

[49] Notter DA, Kouravelou K, Karachalios T, Daletou MK, Haberland NT. Life cycle assessment of PEM FC applications: Electric mobility and μ-CHP. Energy Environ Sci 2015;8(7):1969–85. http://dx.doi.org/10.1039/c5ee01082a.

[50] Keoleian G, Miller S, Kleine RD, Fang A, Mosley J. Life cycle material data update for GREET model - report no. CSS12-12. Tech. rep., 2012, p. 214.

[51] Sherwood SC, Dixit V, Salomez C. The global warming potential of near-surface emitted water vapour. Environ Res Lett 2018;13(10):104006. http://dx.doi.org/10.1088/1748-9326/aae018.

[52] Bradley S, Ducrocq J, Gallarda J, Mineur B, Ott W, Ritter A, et al. Best available techniques for the co-production of hydrogen, carbon monoxide & their mixtures by steam reforming. Tech. rep., Brussels: EUROPEAN INDUSTRIAL GASES ASSOCIATION AISBL; 2013.

[53] Thomas M, Ellingsen LA-W, Hung CR. Research for TRAN Committee - Resource and climate aspects of lithium-ion traction batteries and battery electric vehicles. Brussels: European Parliament, Policy Department for Structural and Cohesion Policies; 2018, http://dx.doi.org/10.2861/944056.